

CDJ-Pontryagin Optimal Control for General Continuously Monitored Quantum Systems

Tathagata Karmakar^{1,2,3,4,5,*} and Andrew N. Jordan^{3,1,2,6,†}

¹*Department of Physics and Astronomy, University of Rochester, Rochester, NY 14627, USA*

²*Center for Coherence and Quantum Optics, University of Rochester, Rochester, NY 14627, USA*

³*Institute for Quantum Studies, Chapman University, Orange, CA, 92866, USA*

⁴*Department of Chemistry, University of California, Berkeley, California 94720, USA*

⁵*Berkeley Center for Quantum Information and Computation, Berkeley, California 94720, USA*

⁶*The Kennedy Chair in Physics, Chapman University, Orange, CA 92866, USA*

(Dated: April 18, 2025)

The Chantasri-Dressel-Jordan (CDJ) stochastic path integral formalism (Chantasri et al. 2013 and 2015) characterizes the statistics of the readouts and the most likely conditional evolution of a continuously monitored quantum system. In our work, we generalize the CDJ formalism to arbitrary continuously monitored systems by introducing a costate operator. We then prescribe a generalized Pontryagin’s maximum principle for quantum systems undergoing arbitrary evolution and find conditions on optimal control protocols. We show that the CDJ formalism’s most likely path can be cast as a quantum Pontryagin’s maximum principle, where the cost function is the readout probabilities along a quantum trajectory. This insight allows us to derive a general optimal control equations for arbitrary control parameters to achieve a given task. We apply our results to a monitored oscillator in the presence of a parametric quadratic potential and variable quadrature measurements. We find the optimal potential strength and quadrature angle for fixed-end point problems. The optimal parametric potential is analytically shown to have a “bang-bang” form. We apply our protocol to three quantum oscillator examples relevant to Bosonic quantum computing. The first example considers a binomial codeword preparation from an error word, the second example looks into cooling to the ground state from an even cat state, and the third example investigates a cat state to cat state evolution. We compare the statistics of the fidelities of the final state with respect to the target state for trajectories generated under the optimal control with those generated under a sample control. Compared to the latter case, we see a 40-196% increase in the number of trajectories reaching more than 95% fidelities under the optimal control. Our work provides a systematic prescription for finding quantum optimal control for continuously monitored systems.

I. INTRODUCTION

Near-term quantum hardware needs high-fidelity state preparation or stabilization schemes [1]. State preparation schemes are required for tasks such as encoding error correcting codes [2], running quantum algorithms, performing simulations [3, 4], etc. To that end, a promising approach is dissipation engineering. The idea is to utilize a carefully designed system-environment interaction as a resource for quantum computation [5, 6]. Experiments have utilized dissipation engineering to prepare quantum states [7, 8], stabilize quantum states [9, 10], produce entangled states [11, 12], perform autonomous quantum error correction [13, 14], etc. However, finding optimal control for such tasks can be challenging [15].

In this article, we investigate optimal control protocols for quantum systems undergoing measurements. Quantum measurements are performed by monitoring the environment coupled to a quantum system [16, 17]. When the system-environment coupling is weak, and the environment is measured in small successive time intervals, quasi-continuous monitoring of the quantum system is

realized. In this scenario, the system’s evolution conditioned on the measurement readouts is stochastic. The sequence of readouts and associated conditional state evolution realizes a quantum trajectory [17–19]. Continuous measurements allow real-time tracking of a quantum state. Such measurements have been utilized in a diverse set of scenarios such as qubit state monitoring [20, 21], remote entanglement generation [22, 23], Zeno dragging of a qubit [24], monitoring of trapped atoms [25], quantum sensing [26, 27], etc. Continuous-monitoring-based theoretical investigations into entangling measurements [28–30], quantum state estimation [31], quantum state smoothing [32, 33], parameter estimation [34, 35], tomography [36] have been done. The readout in a continuous measurement can be used for feedback control of the monitored system [37, 38]. With continuous feedback, cooling of an atom trapped in a cavity [39], catching and reversing a quantum jump [40], continuous quantum error correction [41] have been achieved. In our work, we consider quantum optimal control for continuously monitored systems. For simplicity, the control parameters in our analysis correspond to either a tunable system-environment interaction (i.e., quadrature of a homodyne readout) or the strength of a drive applied to the system. To find optimal control protocols, we generalize the Chantasri-Dressel-Jordan (CDJ) stochastic path integral approach.

* tatha@berkeley.edu

† jordan@chapman.edu

The CDJ formalism expresses the probability densities of the quantum trajectories of a continuously monitored system in terms of a path integral of the exponential of a stochastic action [42–44]. The stochastic action is functional of the readouts, a set of coordinates characterizing the quantum state (e.g. Bloch coordinates for a qubit), and a corresponding set of auxiliary variables. One can extremize the stochastic action to find the most likely readouts. The corresponding trajectories are called most likely paths (MLP) or optimal paths (OP). We can express the most likely evolution in terms of Hamilton’s equations between state coordinates and the auxiliary variables. Thus, the CDJ formalism provides a classical-like description of continuously monitored systems. The CDJ stochastic path integral approach has led to insights into fluorescence from superconducting qubits [45, 46], multiple MLPs [47], onset of chaos for a qubit undergoing simultaneous monitoring of non-commuting observables [48], geometric phase [49], entanglement evolution [50]. The CDJ formalism has shown success in studying monitored superconducting qubits [51], quantum caustics in fluorescing qubits [52], measurement induced remote entanglement generation [53]. Previously, we extended the CDJ stochastic path integral approach to continuous variable systems [54]. Namely, to a simple harmonic oscillator in general Gaussian states undergoing simultaneous continuous position and momentum measurements. Under steady-state assumption, we analytically solved for the optimal paths and confirmed our results with simulated trajectories. Recent investigations suggest that state preparation using the most likely paths for noisy quantum systems can lead to higher success rates than the Lindbladian master equation [55]. Lewalle et al. connected Pontryagin optimal control and the CDJ formalism for qubits undergoing non-Hermitian dynamics [56]. The Pontryagin maximum principle provides a strategy for optimal control under constrained evolution by introducing costate parameters [57]. Utilizing this connection, the optimality of the shortcut to Zeno approaches (with counter-diabatic driving) for Zeno dragging of a qubit was shown [58].

Despite such successes, the CDJ stochastic path integral approach does have drawbacks. Construction of the stochastic action uses a parametrization of the state of the quantum system in terms of a finite number of variables (e.g. Bloch coordinates of a qubit or position and momentum expectation values of an oscillator). This can be a severe limitation for many-body systems or continuous variable systems in non-Gaussian states. In this work, we overcome this limitation by providing a stochastic action principle for general continuously monitored systems. We achieve this by taking inspiration from the Pontryagin maximum principle and introducing a costate operator. Such a costate-based description was also prescribed in the appendix of Ref. [45]. Here, we first reproduce our previous most likely path work for Gaussian states of a harmonic oscillator. Then, we provide a general formulation of the Pontryagin’s maximum principle

that aims to optimize a cost functional constrained on the evolution of a quantum system under control. We derive the Chantasri-Dressel-Jordan formalism as a special case of general Pontryagin’s maximum principle. Next, we look at the case of a quantum harmonic oscillator in the presence of a parametric quadratic potential and undergoing variable quadrature measurements. For this system, we analytically find the optimal parametric potential strength and measurement quadrature under fixed-endpoint constraints. The optimal parametric potential is found to be of “bang-bang” form. We look at three different state preparation examples. First, we look at the preparation of the binomial code word $\frac{|0\rangle+|4\rangle}{\sqrt{2}}$ starting from the state $\frac{|0\rangle-|4\rangle}{\sqrt{2}}$. The initial state corresponds to an error word under no jump evolution [2, 59]. This example is relevant for error correction of Bosonic codes. In the second example, we look at cooling to the ground state, starting from a cat state [60]. In this case, we are looking into the problem of parametric cooling [61, 62] although we do not include feedback. The results are relevant for the ground state preparation of oscillators [63, 64]. As our third example, we look at a cat state to cat state evolution where the sizes are $|\alpha|^2 \sim 2.4$. In all three cases, we construct a sample control that can also help us reach the target state. We then generate 10,000 stochastic trajectories each under the optimal and the sample control. For each type of control, we look at the histograms of the fidelities of the final state with respect to the target state. We find, compared to the sample control, the optimal control leads to a 40-196% increase in the number of trajectories reaching more than 95% fidelity. The results show that optimal controls found under the fixed-endpoints assumptions can still be helpful in state preparation. We stress that although we restrict the examples to a continuously monitored harmonic oscillator, the general principles presented are applicable beyond monitored quantum systems.

The utility of the costate formalism for finding quantum optimal control of open quantum systems is known [65]. Using the Pontryagin maximum principle, the optimality of quantum annealing (QA) and quantum approximate optimization algorithm (QAOA) has been investigated [66]. The costate-based approach has helped optimize transmon readout as well [67]. However, such a general framework for continuously monitored systems was lacking. Here, we state the Pontryagin maximum principle for optimizing a general cost function constrained on a quantum system undergoing arbitrary evolution. We also provide the equation for the evolution of the costate operator. In past investigations on open quantum systems, the costate evolution equation was found to be the negative conjugate of the state evolution equation [65, 66]. We achieve a more complicated and nonlinear relationship between the state and costate evolutions for the general case. Using the general principles, we derive the equations for optimal paths and the optimal control protocols for continuously monitored systems as a special

case. We also show that under an operator transformation, we can reduce the costate evolution equation to be the negative conjugate of the state evolution. Such simplification might not follow for the general cost functions.

Optimal control protocols play crucial roles in designing fault-tolerant architectures. On the other hand, algorithms on NISQ devices can benefit from optimal control. In other words, quantum optimal control protocols can bridge these two paradigms of fault-tolerant quantum computation [68]. The Pontryagin maximum principle has been applied to variational quantum algorithms where the optimality of “bang-bang” protocols has been shown [69]. Other problems where the principle has been employed include maximally entangled state preparation [70] and Grover’s search algorithm [71]. Another recent example includes pulse optimization in circuit-QED systems [72]. Our analysis can serve as a precursor for a systematic investigation into quantum optimal control protocols for running quantum algorithms with diffusive measurements [73].

We restrict our attention to a monitored harmonic oscillator as it provides a suitable description of a wide range of systems. These include mirrors, membranes, optical degrees of freedom, superconducting resonators, and so on. Mechanical resonators can be monitored by clamping them in a cavity and performing homodyne measurements on the transmitted light [63, 74–76]. Both theoretical and experimental investigations into oscillator monitoring [19, 38, 76–86], and feedback control [63, 87–91] have been done. Explorations involving mechanical resonators include the generation of superposition states [92], squeezed states [93–97], resonator-resonator entanglement [98, 99], optical field-resonator entanglement [100, 101], etc. Another form of resonators involves superconducting cavities [102]. They have been used to realize dual-rail encoding of a logical qubit. In this case, logical measurements are performed by mapping the state of a superconducting cavity to an ancilla transmon and performing a dispersive readout of the transmon [103, 104]. Investigations into building quantum random access memory architecture [105] and performing quantum error correction [106, 107] with 3D superconducting cavities have been done. Nonlinear optical systems have also seen rapid progress. With such systems, the onset of non-Gaussian physics [108, 109], quantum nondemolition measurement of photon numbers and approximate GKP state preparation [110], Hamiltonian engineering [111], cubic phase gate implementation [112] have been studied. Therefore, the examples discussed in our work are relevant to a broad set of ongoing investigations.

This paper is organized as follows. In section II, we describe the stochastic evolution of a monitored quantum system, provide a brief introduction to the Chantasri-Dressel-Jordan stochastic path integral formalism, construct the stochastic Hamiltonian for a general monitored system, and verify the optimal paths predicted by the general formalism with previous results for a monitored harmonic oscillator. Section III formulates the Pontryagin’s

maximum principle for a general quantum system and rederives the general CDJ formalism as a special case. Section III also looks at the optimal control problem for a monitored oscillator, provides associated equations to be solved, and analyzes three examples. Lastly, we conclude in section IV.

II. STOCHASTIC EVOLUTION OF THE SYSTEM

In this section, we look at the conditional stochastic evolution of a continuously monitored quantum system. Consider a system with Hamiltonian \hat{H} ¹. Assume, the system is coupled to a detector which allows us to monitor an observable \hat{L} (see Fig. 1). We further assume that the measurement Kraus operators [17, 113] are of Gaussian form

$$\hat{M}(r) = \left(\frac{dt}{2\pi\tau}\right)^{\frac{1}{4}} \exp\left[-\frac{dt}{4\tau}(r\mathbb{1} - \hat{L})^2\right], \quad (1)$$

where τ signifies the collapse timescale of the measurement. The state of the system is expressed by the density matrix $\hat{\rho}$. The Stratonovich stochastic master equation expressing the conditional dynamics of the systems under continuous monitoring is [18, 19]

$$\begin{aligned} \frac{\partial \hat{\rho}}{\partial t} &= \hat{\mathfrak{F}}_{\hat{\rho}}(\hat{\rho}, r) \\ &= -i[\hat{H}, \hat{\rho}] - \frac{1}{4\tau} [\Delta \hat{V}, \hat{\rho}]_+ + \frac{1}{2\tau} r [\Delta \hat{L}, \hat{\rho}]_+, \end{aligned} \quad (2)$$

where we define $\hat{V} = \hat{L}^2$, and $[\dots, \dots]_+$ denotes the anticommutator. $\Delta \hat{O} = \hat{O} - \langle \hat{O} \rangle$, for any operator \hat{O} . The subscript $\hat{\rho}$ on $\hat{\mathfrak{F}}$ denotes the nonlinear nature of the equation. In the subsequent analysis, we will assume \hat{L} is Hermitian and there is a single measurement channel. The results presented can be easily generalized to non-Hermitian observables or multiple measurement channels. The readout r obtained in time dt is

$$r = \langle \hat{L} \rangle + \sqrt{\tau} \frac{dW}{dt}. \quad (3)$$

Here, dW is a Wiener noise such that $dW^2 = dt$ [114, 115].

Eq. (2) quantifies the stochastic evolution of the system conditioned on the stochastic readout r . Note that Eq. (2) can describe stochastic unravelings of an unmonitored system too [116]. In the subsequent sections, we characterize the statistics of the readouts.

¹ We assume $\hbar = 1$ throughout the analysis.

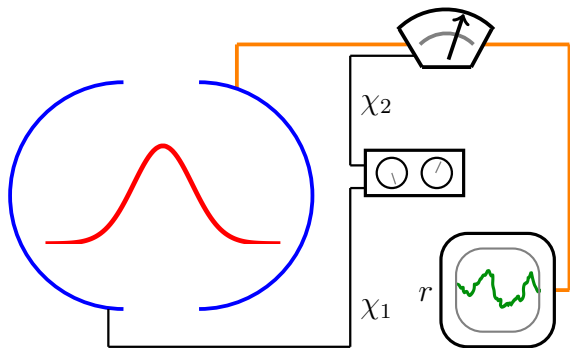


FIG. 1. We sketch the schematic of a quantum system coupled to a detector that monitors the system. The readout r obtained due to continuous measurement is noisy. In general, the system is controlled through a parameter χ_1 that changes the system Hamiltonian (unitary control) and another parameter χ_2 that modifies the measurements (dissipative control) performed on the system.

A. CDJ formalism: Stochastic action and Hamiltonian

Now, we provide a brief introduction to the Chantasri-Dressel-Jordan (CDJ) formalism. The CDJ stochastic path integral approach expresses the probability density of realizing a particular quantum trajectory in terms of a path integral of the exponential of a stochastic action [42–44]. This formalism characterizes the statistics of the continuous measurements. By extremizing the stochastic action, most likely dynamics of the system are obtained. Such most likely dynamics (also called the most likely paths or optimal paths) can be expressed in terms of a Hamiltonian that incorporates both the unitary dynamics and the dissipative dynamics due to measurement. Thus, we obtain a classical-like description of monitored quantum systems.

In the CDJ stochastic path integral approach, we parametrize Eq. (2) in terms of coordinates \mathbf{q} . Here, the coordinates represent the state of the system. For example, they can be the Bloch coordinates for a qubit [53] or the quadrature expectation values for an oscillator in a coherent state [54]. Assume the initial state of the system is $\mathbf{q}(t=0) = \mathbf{q}_i$ and the trajectories are postselected such that the final state is $\mathbf{q}(t=t_f) = \mathbf{q}_f$. The system is monitored dt intervals. The CDJ stochastic path integral approach expresses the probability density of realizing intermediate states $\{\mathbf{q}\}$ and readouts $\{r\}$ in the limit $dt \rightarrow 0$ as [54]

$$\mathcal{P} = \int \mathcal{D}\mathbf{p} e^{\mathcal{S}} = \int \mathcal{D}\mathbf{p} \exp \left[\int_0^{t_f} dt (-\mathbf{p} \cdot \dot{\mathbf{q}} + \mathcal{H}(\mathbf{p}, \mathbf{q}, r)) \right], \quad (4)$$

where \mathbf{p} are variables conjugate to \mathbf{q} . $\mathcal{H}(\mathbf{p}, \mathbf{q}, r)$, also called the stochastic Hamiltonian, is a functional of

$\{\mathbf{p}, \mathbf{q}, r\}$. The stochastic Hamiltonian is of the form

$$\mathcal{H}(\mathbf{q}, \mathbf{p}, r) = \mathbf{p}^\top \cdot \mathcal{F}(\mathbf{q}, r) + \mathcal{G}(\mathbf{q}, r), \quad (5)$$

where $\dot{\mathbf{q}} = \mathcal{F}(\mathbf{q}, r)$ is the stochastic master equation (2), expressed in terms of the coordinates \mathbf{q} . The second term, $\mathcal{G}(\mathbf{q}, r)$ relates to the conditional probability of readout r as measurements are performed on the system in state \mathbf{q} in interval dt . In other words, $P(r|\mathbf{q}) \sim e^{\Delta t \mathcal{G}(\mathbf{q}, r)}$. The most likely paths (MLP) or optimal paths (OP) can be found by variational extremization of the stochastic action. The equations for the optimal paths are given by [42]

$$\partial_r \mathcal{H} = 0, \quad \dot{\mathbf{q}} = \partial_{\mathbf{p}} \mathcal{H}, \quad \dot{\mathbf{p}} = -\partial_{\mathbf{q}} \mathcal{H}. \quad (6)$$

Define the optimal readout obtained from the first equation above to be $r^*(\mathbf{p}, \mathbf{q})$. The second equation then satisfies $\dot{\mathbf{q}} = \mathcal{F}(\mathbf{q}, r^*)$, consistent with the stochastic master equation. The CDJ formalism has been applied to monitored qubits [45, 51], entangled qubits [53], monitored oscillators in general Gaussian states [54]. The construction of the CDJ stochastic action requires explicit parametrization of the system in terms of a finite number of variables. This might be hard to achieve for many-body systems with very high dimensions or continuous variable systems in non-Gaussian states. In the following formulation, we bypass the need for such parametrization by expressing the most likely evolution in terms of the density matrix.

Eqs. (6) can be interpreted as the extremization of the readout probabilities constrained on the conditional stochastic evolution of \mathbf{q} [58]. The auxiliary variables \mathbf{p} in Eq. (5) act as Lagrange multipliers. We utilize these ideas to construct the stochastic Hamiltonian and action for a general continuously monitored system. If the system state at the beginning of a measurement is $\hat{\rho}$, the probability density of obtaining readout r can be expressed as

$$P(r|\hat{\rho}) = \text{Tr} \left(\hat{M}(r) \hat{\rho} \hat{M}^\dagger(r) \right), \quad (7)$$

where $\hat{M}(r)$ is defined in Eq. (1). We consider the weak measurement limit $dt \ll \tau$ such that the probability density in Eq. (7) can be approximated as

$$P(r|\hat{\rho}) \approx \left(\frac{dt}{2\pi\tau} \right)^{\frac{1}{2}} \left[1 - \frac{dt}{2\tau} \left(r^2 - 2r \langle \hat{L} \rangle + \langle \hat{L}^2 \rangle \right) \right]. \quad (8)$$

Like the auxiliary variables \mathbf{p} we introduce a Hermitian operator $\hat{\sigma}$ and generalize Eq. (5) to define the stochastic Hamiltonian as [117]

$$\mathcal{H} dt \sim \text{Tr} \left(\hat{\sigma} \hat{\mathfrak{F}}_{\hat{\rho}}(\hat{\rho}, r) dt \right) + \ln P(r|\hat{\rho}). \quad (9)$$

The operator $\hat{\sigma}$ is called the costate. As mentioned before, such costate based description for the optimal control of open quantum systems has been adopted in the past [45, 65, 66]. Ignoring multiplicative constants and

using the approximation in Eq. (8), the stochastic Hamiltonian takes the following form

$$\mathcal{H}(\hat{\sigma}, \hat{\rho}, r) = \text{Tr} \left(\hat{\sigma} \hat{\mathfrak{F}}_{\hat{\rho}}(\hat{\rho}, r) \right) - \frac{1}{2\tau} \left(r^2 - 2r \langle \hat{L} \rangle + \langle \hat{L}^2 \rangle \right). \quad (10)$$

The stochastic action can be written as

$$\mathcal{S} = \int_0^{t_f} dt \left(-\text{Tr} \left(\hat{\sigma} \frac{\partial \hat{\rho}}{\partial t} \right) + \mathcal{H} \right). \quad (11)$$

The most likely path under continuous measurements, also called the optimal paths, can be found by the variational extremization of the stochastic action $\delta \mathcal{S} = 0$.

Then, the optimal readout is given by (see Appendix A)

$$r^* = \langle \hat{L} \rangle + \frac{1}{2} \left\langle \left[\Delta \hat{L}, \hat{\sigma} \right]_+ \right\rangle = \langle \hat{L} \rangle + u. \quad (12)$$

The first term denotes the signal. The second term $u = \frac{1}{2} \left\langle \left[\Delta \hat{L}, \hat{\sigma} \right]_+ \right\rangle$ denotes the optimal noise. The equations for the optimal path are given by (see Appendix A)

$$\begin{aligned} \frac{\partial \hat{\rho}}{\partial t} &= -i[\hat{H}, \hat{\rho}] - \frac{1}{4\tau} \left[\Delta \hat{V}, \hat{\rho} \right]_+ + \frac{r^*}{2\tau} \left[\Delta \hat{L}, \hat{\rho} \right]_+, \\ \frac{\partial \hat{\sigma}}{\partial t} &= -i[\hat{H}, \hat{\sigma}] + \frac{1}{4\tau} \left[\Delta \hat{V}, \hat{\sigma} \right]_+ - \frac{r^*}{2\tau} \left[\Delta \hat{L}, \hat{\sigma} \right]_+. \end{aligned} \quad (13)$$

where we choose $\langle \hat{\sigma} \rangle = 1$. We can always make this choice since Eq. (2) preserves the trace. Therefore, adding a scalar to $\hat{\sigma}$ does not change the stochastic Hamiltonian in Eq. (10). Note that, the costate evolution along the optimal path is given by the negative conjugate of the state evolution. In other words,

$$\frac{\partial \hat{\sigma}}{\partial t} = -\hat{\mathfrak{F}}_{\hat{\rho}}^\dagger(\hat{\sigma}, r^*), \quad (14)$$

which may be interpreted as the time reversal of the state evolution. This is consistent with past work using the costate formalism [65]. We will shortly derive a more general expression for the costate evolution where such correspondence might not be valid. The optimal Hamiltonian $\mathcal{H}^*(\hat{\sigma}, \hat{\rho}) = \mathcal{H}(\hat{\sigma}, \hat{\rho}, r^*)$ is given by

$$\begin{aligned} \mathcal{H}^*(\hat{\sigma}, \hat{\rho}) &= \langle i[\hat{H}, \hat{\sigma}] \rangle + \frac{1}{8\tau} \left\langle \left[\Delta \hat{L}, \hat{\sigma} \right]_+ \right\rangle^2 \\ &\quad - \frac{1}{4\tau} \left\langle \left[(\Delta \hat{L})^2, \hat{\sigma} \right]_+ \right\rangle \\ &= \langle i[\hat{H}, \hat{\sigma}] \rangle + \frac{1}{8\tau} \left\langle \left[\hat{L}, \hat{\sigma} \right]_+ \right\rangle^2 \\ &\quad - \frac{1}{4\tau} \left\langle \left[\hat{V}, \hat{\sigma} \right]_+ \right\rangle. \end{aligned} \quad (15)$$

Equations (13) are the equations for the optimal path of a general continuously monitored system. Such formalism can be applied to finite dimensional systems such

as qubits [102], qudits [118], many-body systems [119], and also to continuous variable systems [120], multimode physics in ultrafast optics [108, 109].

Thus, we have provided a costate-based description of the CDJ most likely paths. Our subsequent analysis focuses on the monitored harmonic oscillator.

B. Example : optimal paths of a continuously monitored quantum harmonic oscillator

We consider a quantum harmonic oscillator with Hamiltonian².

$$\hat{H} = \frac{1}{2} \left(\hat{X}^2 + \hat{P}^2 \right), \quad (16)$$

where \hat{X} and \hat{P} are dimensionless position and momentum observables. We consider adaptive measurements of the quadrature given by

$$\hat{L}_\theta = \cos \theta(t) \hat{X} + \sin \theta(t) \hat{P}, \quad (17)$$

where $\theta(t)$ is in general a control parameter. The conjugate quadrature is

$$\hat{M}_\theta = -\sin \theta(t) \hat{X} + \cos \theta(t) \hat{P}. \quad (18)$$

Such measurements are realized by clamping a mechanical oscillator in a cavity and performing a balanced homodyne detection on transmitted light [63, 74–76]. The measurement collapse timescale τ in this case is the inverse of measurement rate and depends on the cavity decay rate, cavity resonator optomechanical field enhanced coupling strength, and detection efficiency [76, 117]. In this article, we assume completely efficient detectors.

The Stratonovich stochastic master equation for the conditional evolution of the monitored oscillator is given by

$$\begin{aligned} \frac{\partial \hat{\rho}}{\partial t} &= \hat{\mathfrak{F}}_\theta(\hat{\rho}, r) \\ &= -i[\hat{H}, \hat{\rho}] - \frac{1}{4\tau} \left[\Delta \hat{V}_\theta, \hat{\rho} \right]_+ + \frac{1}{2\tau} r \left[\Delta \hat{L}_\theta, \hat{\rho} \right]_+, \end{aligned} \quad (19)$$

with the readout $r = \langle \hat{L}_\theta \rangle + \sqrt{\tau} \frac{dW}{dt}$. The optimal paths for the monitored harmonic oscillator in general Gaussian states have been analyzed previously [54]. Subsequent analysis looks at the optimal path for general states.

² In the subsequent analysis, the time and the collapse timescale τ is in units of $1/\omega$, i.e., in terms of the inverse of the oscillator frequency. The quadratures are made dimensionless by scaling position and momentum by $\sqrt{m\omega/\hbar}$ and $\frac{1}{\sqrt{\hbar m\omega}}$ respectively (see Ref. [54]). Then, the stochastic readout is dimensionless as well.

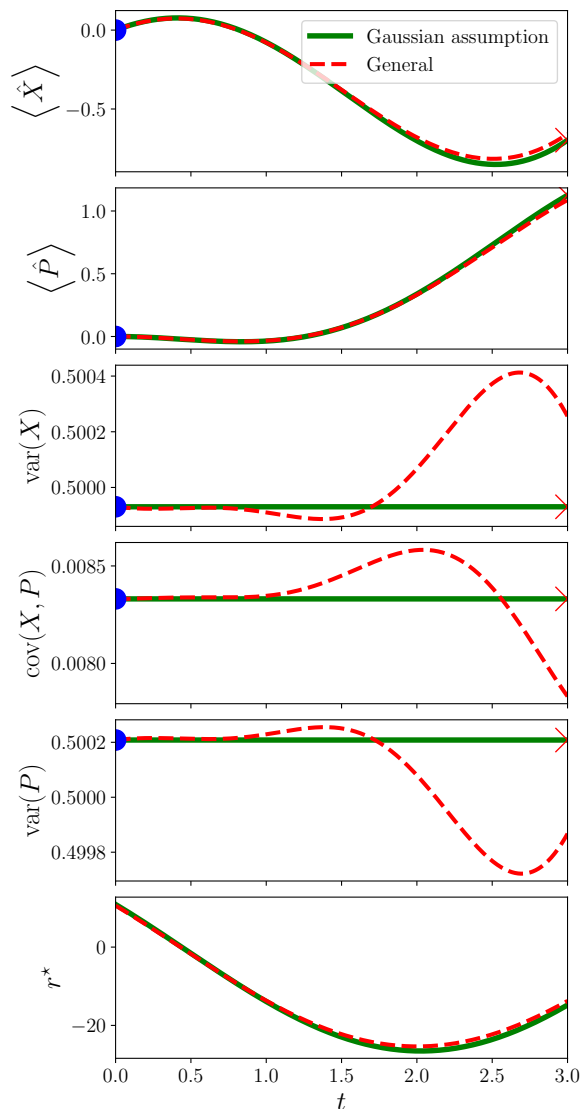


FIG. 2. The plots show the optimal path for Gaussian states under position measurements (i.e. $\theta = 0$). The top two panels show the time evolution of the position and momentum expectation values. The next three panels show the time evolution of the position variance, the covariance of the position and momentum, and the momentum variance. The final panel shows the most likely readout obtained as a function of time. All the observables are scaled to be dimensionless (see Sec. II B). The time and the collapse timescale ($\tau = 15.0$) are in units of the inverse of the oscillator frequency. In the plots, the green curve shows evolution obtained from Ref. [54], with a Gaussian state assumption. The red dashed lines show the most likely path obtained from the general formalism presented in sec. II C. The blue dots in the first five panes denote the initial ,and the red crosses denote the final state. The initial state is a squeezed vacuum state, and the final state is a squeezed coherent state. The squeezing is determined by the τ (see Appendix I). We see that the expectation values match very well. Since we make a steady state assumption (see Ref. [54]), the variances and covariances do not show any evolution for Gaussian state formalism. The general optimal path, on the other hand, shows a slight deviation from the final state, signifying that only position measurements are not sufficient to reach the final state completely. Such deviation brings out the failure of the steady-state assumption.

C. Optimal readout and paths

Following the analysis in Sec. II A, we now characterize the most likely readouts and path of the monitored oscillator. The expression for the optimal readout is

$$r^* = r_\theta = \frac{1}{2} \left\langle \left[\hat{L}_\theta, \hat{\sigma} \right]_+ \right\rangle. \quad (20)$$

The equations for the optimal paths are

$$\frac{\partial \hat{\rho}}{\partial t} = -i[\hat{H}, \hat{\rho}] - \frac{1}{4\tau} \left[\Delta \hat{V}_\theta, \hat{\rho} \right]_+ + \frac{1}{2\tau} r_\theta \left[\Delta \hat{L}_\theta, \hat{\rho} \right]_+, \quad (21a)$$

$$\frac{\partial \hat{\sigma}}{\partial t} = -i[\hat{H}, \hat{\sigma}] + \frac{1}{4\tau} \left[\Delta \hat{V}_\theta, \hat{\sigma} \right]_+ - \frac{1}{2\tau} r_\theta \left[\Delta \hat{L}_\theta, \hat{\sigma} \right]_+. \quad (21b)$$

We see that $\hat{\sigma}$ influences the evolution of the state only through the optimal readout r_θ , which is a real scalar. We can reduce the problem's dimensionality significantly by looking at the evolution of r_θ only. Similar to Eq. (20), we define the scalar v_θ in terms of the conjugate quadrature as

$$v_\theta = \frac{1}{2} \left\langle \left[\hat{M}_\theta, \hat{\sigma} \right]_+ \right\rangle. \quad (22)$$

We also adopt the following definitions,

$$w_\theta = i \left\langle \left[\hat{\sigma}, \hat{L}_\theta \right] \right\rangle, \quad z_\theta = i \left\langle \left[\hat{\sigma}, \hat{M}_\theta \right] \right\rangle. \quad (23)$$

We can now express the evolution of the optimal readout in terms of the following coupled equations (see Appendix C)

$$\frac{dr_\theta}{dt} = \dot{\phi} v_\theta \quad (24a)$$

$$\frac{dv_\theta}{dt} = -\dot{\phi} r_\theta + \frac{w_\theta}{4\tau} \quad (24b)$$

$$\frac{dw_\theta}{dt} = \dot{\phi} z_\theta, \quad \frac{dz_\theta}{dt} = -\dot{\phi} w_\theta, \quad (24c)$$

where $\dot{\phi} = \dot{\theta} + 1$. Note, the $\dot{\theta}$ in the definition of $\dot{\phi}$ arises due to the varying quadrature measurement. The additional 1 is due to the unitary dynamics of the oscillator. By integrating Eqs. (21a) and (24) together, we can find the optimal paths of a monitored harmonic oscillator in arbitrary states. This simplification is advantageous in numerical simulations since, instead of two operators $\hat{\rho}$ and $\hat{\sigma}$, we only need to integrate one operator $\hat{\rho}$ and four scalars. This analysis goes beyond the Gaussian state assumption in Ref. [54].

We assume $\phi(t) = \theta(t) + t$ and $\phi(0) = \theta(0) = 0$ without the loss of generality. Eq. (24c) can be integrated to find

$$\begin{aligned} w_\theta(t) &= A \cos \phi(t) + B \sin \phi(t), \\ z_\theta(t) &= -A \sin \phi(t) + B \cos \phi(t), \end{aligned} \quad (25)$$

where A and B are real constants corresponding to the initial values of w_θ and z_θ . Putting these values into Eqs. (24a) and (24b), we can solve for u_θ and v_θ as

$$r_\theta(t) + iv_\theta(t) = e^{-i\phi(t)} \left(\alpha + \frac{it}{8\tau} (A + iB) + \int_0^t dt' h(t') \right), \quad (26)$$

with

$$h(t) = \frac{i}{8\tau} (A - iB) e^{i2\phi(t)}, \quad (27)$$

and α is a complex number. Solving for the optimal path then involves integrating Eqs. (21a) and (26) from the initial state $\hat{\rho}(0) = \hat{\rho}_i$ and finding the values of α , A , and B such that $\hat{\rho}(t_f) = \hat{\rho}_f$. Thus we have solved for the optimal paths of a monitored simple harmonic oscillator in an arbitrary state. According to Eqs. (24), the optimal readout behaves like a resonantly driven oscillator with frequency $\dot{\phi}$. This is consistent with optimal path solutions previously found for Gaussian states [54]. See Fig. 2 shows that our formalism for general optimal paths reproduces previous results of Gaussian state evolution (see Appendix D for details on the numerical method). Here, the control parameter $\theta(t) = 0$. Note that the covariance matrix elements in the general framework show a slight deviation from the final state. The numerical solution to the general optimal path produces a final state that is very close to the target state. However, the slight deviation signifies the closest we can get to the target state under only position monitoring. The question of the reachability of specific states under available control is interesting, although it is beyond our current endeavor.

Thus, the costate-based analysis of the CDJ most likely paths reproduces the previous coordinate-based results for the monitored oscillator in general Gaussian states. In the subsequent analysis, we will show that the CDJ most likely paths can be derived as a special case of a general Pontryagin's maximum principle.

III. PONTYAGIN MAXIMUM PRINCIPLE FOR THE OPTIMAL CONTROL OF QUANTUM SYSTEMS

We now provide a formal statement for the Pontryagin maximum principle for arbitrary quantum systems. We show that the most likely paths provided by the Chantasri-Dressel-Jordan stochastic path integral formalism can be derived as a special case of the following analysis. We consider quantum systems in state $\hat{\rho}(t)$, with an evolution characterized by

$$\frac{\partial \hat{\rho}}{\partial t} = \mathcal{F}_{\hat{\rho}, \chi}[\hat{\rho}], \quad (28)$$

where the superoperator $\mathcal{F}_{\hat{\rho}, \chi}$ depends on control $\chi(t)$ and the state $\hat{\rho}(t)$. Thus, Eq. (28) is, in general, nonlinear. Further, assume $\mathcal{F}_{\hat{\rho}, \chi}$ depends on $\hat{\rho}$ through expecta-

tation values of different observables such that,

$$\mathcal{F}_{\hat{\rho} + \delta\hat{\rho}, \chi}[\hat{\rho} + \delta\hat{\rho}] = \mathcal{F}_{\hat{\rho}, \chi}[\hat{\rho}] + \mathcal{F}_{\hat{\rho}, \chi}[\delta\hat{\rho}] + \sum_{\nu=0}^{\nu_1} \text{Tr}(\hat{A}_{\nu, \chi} \delta\hat{\rho}) \mathcal{F}_{\hat{\rho}, \chi}^{\nu}[\hat{\rho}], \quad (29)$$

up to first order in $\delta\hat{\rho}$. Here $\hat{A}_{\nu, \chi}$ are Hermitian observables and $\mathcal{F}_{\hat{\rho}, \chi}^{\nu}$ are superoperators for $\nu = 0, \dots, \nu_1$.

For continuously monitored systems, we consider a continuous approximation of the readout r , and Eq. (28) corresponds to the Stratonovich master equation [121, 122]. Without loss of generality, we mathematically treat the readout as a part of the control in this section.

We consider system evolving from $\hat{\rho}(t = t_0) = \hat{\rho}_0$ to $\hat{\rho}(t = t_1) = \hat{\rho}_f$ and introduce the following cost functional that will be minimized

$$J = \int_{t_0}^{t_1} f^0(\hat{\rho}(t), \chi(t)) dt, \quad (30)$$

where t_1 is not fixed. f^0 is an as-yet-unspecified function of the system state and the control. We can express the variation of f^0 as follows

$$f^0(\hat{\rho} + \delta\hat{\rho}, \chi) = f^0(\hat{\rho}, \chi) + \text{Tr} \left(\frac{\delta f^0}{\delta \hat{\rho}} \delta \hat{\rho} \right). \quad (31)$$

We assume the controls are $\chi : [t_0, t_1] \rightarrow U_C$ with $U_C \subset \mathbb{R}^m$ such that the set of $\chi(t)$ for $t_0 \leq t \leq t_1$ has a compact closure in \mathbb{R}^m (i.e. bounded) [123]. In this work, the control is assumed to be piecewise continuous. However, the results apply to a more general class of controls (measurable and bounded, see Ref. [123]). We also assume the cost is a smooth function of the quantum state and the control variables.

Problem statement: For all possible controls $\chi(t)$ that take the system from $\hat{\rho}_0$ to $\hat{\rho}_f$, find the one $\chi^*(t)$ that minimizes the cost in Eq. (30).

We can look at the problem geometrically. We define the variable

$$q^0(t) = \int_{t_0}^t f^0(\hat{\rho}(t), \chi(t)) dt, \quad (32)$$

and an extended coordinate $Q(t) \equiv (q^0(t), \hat{\rho}(t))$. Then, the cost in Eq. (30) is given by $J = q^0(t_1)$. Therefore, we consider all controls $\chi(t)$ that starts from the coordinate $Q(t_0) = (0, \hat{\rho}_0)$ and ends up at the line $Q(t_1) = (q^0(t_1), \hat{\rho}_f)$. Optimal control corresponds to the minimization of the coordinate $q^0(t_1)$ over such controls. We also define the auxiliary variables $P = (p_0, \hat{\sigma})$, where p_0 is a real number and $\hat{\sigma}$ is a Hermitian operator (costate). The auxiliary variables evolve according to

$$\frac{dp_0}{dt} = 0, \quad (33)$$

and

$$\frac{\partial \hat{\sigma}}{\partial t} = -p_0 \frac{\delta f^0}{\delta \hat{\rho}} - \mathcal{F}_{\hat{\rho}, \chi}^\dagger[\hat{\sigma}] - \sum_{\nu=0}^{\nu_1} \hat{A}_{\nu, \chi} \text{Tr}(\hat{\sigma} \mathcal{F}_{\hat{\rho}, \chi}^{\nu}[\hat{\rho}]). \quad (34)$$

We consider the Hamiltonian

$$\mathcal{H}(P, Q, \chi) = p_0 f^0 + \text{Tr}(\hat{\sigma} \mathcal{F}_{\hat{\rho}, \chi}[\hat{\rho}]). \quad (35)$$

With fixed Q and P , we consider the supremum of the above with respect to the control

$$\mathcal{K}(P, Q) = \sup_{\chi \in U_C} \mathcal{H}(Q, P, \chi). \quad (36)$$

The Pontryagin maximum principle [123]: The necessary condition for control $\chi^*(t)$ and trajectory $Q(t)$ to be optimal is \exists a non-zero $P(t)$ corresponding to $\chi^*(t)$ and $Q(t)$ such that (*Condition I*) the function $\mathcal{H}(P(t), Q(t), \chi)$ attains its maximum at $\chi^*(t)$ for almost all $t_0 \leq t \leq t_1$:

$$\mathcal{H}(P(t), Q(t), \chi^*(t)) = \mathcal{K}(P(t), Q(t)). \quad (37)$$

(*Condition II*) At the final time, the following conditions are true:

$$p_0(t_1) \leq 0, \quad (38a)$$

$$\mathcal{K}(P(t_1), Q(t_1)) = 0. \quad (38b)$$

Furthermore, if $P(t)$ satisfies Eqs. (33) and (34), p_0 and \mathcal{K} are constants. Thus, Condition II is satisfied for any $t_0 \leq t \leq t_1$.

The above principle can be proven by following the steps laid out in Ref. [123], with the equations of motion replaced by Eq. (28). Note that the conditions are necessary but not sufficient. One should verify the existence of optimal control before applying the maximum principle. Also, a solution found using the maximum principle might not be optimal when multiple such solutions are possible. Further investigations are required to ensure optimality in such scenarios. If the control $\chi(t)$ is piecewise continuous, like in our considerations, Condition I is satisfied everywhere. Also, for a fixed time interval, the constraint specified by Eq. (38b) is lifted.

For variable end points : The end points $\hat{\rho}_0$ and $\hat{\rho}_f$ might not be fixed and can belong to manifolds \mathcal{M}_0 and \mathcal{M}_f of dimensions r_0 and r_f , respectively. Assume $\hat{\rho}(t)$ is the corresponding optimal solution. Also, assume $T_{\hat{\rho}(t_0)}\mathcal{M}_0$ and $T_{\hat{\rho}(t_1)}\mathcal{M}_f$ are tangent spaces of \mathcal{M}_0 and \mathcal{M}_f at $\hat{\rho}(t_0)$ and $\hat{\rho}(t_1)$ respectively. The tangent spaces have dimensions r_0 and r_f , too. Then, for optimal control, the following holds:

Condition III or the transversality condition: If $\Delta\hat{\rho}_0 \in T_{\hat{\rho}(t_0)}\mathcal{M}_0$ and $\Delta\hat{\rho}_f \in T_{\hat{\rho}(t_1)}\mathcal{M}_f$, then

$$\text{Tr}(\hat{\sigma}(t_0)\Delta\hat{\rho}_0) = 0, \quad (39a)$$

$$\text{Tr}(\hat{\sigma}(t_f)\Delta\hat{\rho}_f) = 0. \quad (39b)$$

We will only consider the fixed-endpoint problems in this article for simplicity.

Therefore, we described a general Pontryagin's maximum principle for quantum systems undergoing arbitrary dynamics.

A. Optimal control in continuously monitored systems

Now, we apply the above results to continuously monitored systems,

$$\frac{\partial \hat{\rho}}{\partial t} = \hat{\mathfrak{F}}_{\hat{\rho}}(\hat{\rho}, r), \quad (40)$$

where r is the readout. We consider trajectories with initial state $\hat{\rho}(0) = \hat{\rho}_0$ and final state $\hat{\rho}(t_f) = \hat{\rho}_f$. We divide the total interval $[0, t_f]$ into small intervals of length Δt such that $n\Delta t = t_f$. Assume we obtain readouts r_0, r_1, \dots, r_{n-1} in each Δt interval. Using Eq. (40), we can update the corresponding quantum state conditionally to $\hat{\rho}_0, \hat{\rho}_1, \dots, \hat{\rho}_{n-1}, \hat{\rho}_n = \hat{\rho}_f$. Then the probability density of obtaining the set of readouts $\{r_k\} = r_0, r_1, \dots, r_{n-1}$, with initial state $\hat{\rho}_0$ is [42, 54]

$$P(r_{n-1}, \dots, r_2, r_1, r_0 | \hat{\rho}_0) = P(r_{n-1}, \dots, r_2, r_1 | r_0, \hat{\rho}_0) P(r_0, | \hat{\rho}_0). \quad (41)$$

Now, from Eqs. (7) and (8), we can approximate (up to first order in Δt) the second term on the right hand side as

$$P(r_0 | \hat{\rho}_0) \approx \Gamma_{\Delta t} e^{-\frac{\Delta t}{2\tau}(r_0^2 - 2r_0 \langle \hat{L} \rangle + \langle \hat{L}^2 \rangle)}, \quad (42)$$

where $\Gamma_{\Delta t}$ is a constant. The condition of initial state $\hat{\rho}_0$ and obtaining readout r_0 in the first term is the same as considering the state $\hat{\rho}_1$ at $t = \Delta t$ for Markovian dynamics. Thus,

$$P(r_{n-1}, \dots, r_2, r_1, r_0 | \hat{\rho}_0) = P(r_{n-1}, \dots, r_2, r_1 | \hat{\rho}_1) \times \Gamma_{\Delta t} e^{-\frac{\Delta t}{2\tau}(r_0^2 - 2r_0 \langle \hat{L} \rangle + \langle \hat{L}^2 \rangle)}. \quad (43)$$

Carrying out such decomposition and taking the limit $\Delta t \rightarrow 0$, the probability density of obtaining a specific set of readouts (thus, realizing a specific trajectory) is

$$P(r(t) | \hat{\rho}_0) = \tilde{\Gamma}_{\Delta t} e^{-\int_0^{t_f} \frac{dt}{2\tau}(r^2 - 2r \langle \hat{L} \rangle + \langle \hat{L}^2 \rangle)}, \quad (44)$$

which is a functional of the trajectory. The most likely trajectory is obtained by maximizing the argument of the exponent or, equivalently, minimizing the functional

$$J = \int_0^{t_f} \frac{dt}{2\tau} \left(r^2 - 2r \langle \hat{L} \rangle + \langle \hat{L}^2 \rangle \right). \quad (45)$$

Thus, for continuously monitored systems we can identify

$$f^0(\hat{\rho}, r, \chi) = \frac{1}{2\tau} \left(r^2 - 2r \langle \hat{L}_\chi \rangle + \langle \hat{L}_\chi^2 \rangle \right) \quad (46)$$

from Eq. (30), where we take the possible control χ dependence of the monitored observable into account. To apply the Pontryagin's maximum principle, we construct the stochastic Hamiltonian

$$\mathcal{H}(p_0, \hat{\sigma}, \hat{\rho}, r, \chi) = p_0 f^0(\hat{\rho}, r, \chi) + \text{Tr}(\hat{\sigma} \hat{\mathfrak{F}}(\hat{\rho}, r)). \quad (47)$$

From Condition II and Eq. (33), we see that $p_0 \leq 0$ and $p_0 = \text{const}$. In this article, we ignore the abnormal optimal ($p_0 = 0$) therefore, $p_0 < 0$. Note that multiplying \mathcal{H} by a constant only changes the adjoint coordinate $P(t) = (p_0, \hat{\sigma})$ by a constant factor. There is no change in the most likely path evolutions and the optimal control conditions. Hence, we can choose $p_0 = -1$ such that the stochastic Hamiltonian becomes

$$\mathcal{H}(\hat{\sigma}, \hat{\rho}, r, \chi) = -f^0(\hat{\rho}, r, \chi) + \text{Tr}(\hat{\sigma}\hat{\mathfrak{F}}(\hat{\rho}, r)). \quad (48)$$

In this case, from the variation of the stochastic master equation, we get the following equations

$$\begin{aligned} \hat{A}_{0,\chi} &= \frac{1}{2\tau}\hat{L}_\chi^2, & \mathcal{F}_{\hat{\rho},\chi}^0 &= \hat{\mathbb{1}}, \\ \hat{A}_{1,\chi} &= -\frac{r}{\tau}\hat{L}_\chi, & \mathcal{F}_{\hat{\rho},\chi}^1 &= \hat{\mathbb{1}}, \end{aligned} \quad (49)$$

where $\hat{\mathbb{1}}$ denotes the identity operator. Also, from the variation of f^0

$$\frac{\partial f^0}{\partial \hat{\rho}} = \frac{1}{2\tau} \left(-2r\hat{L}_\chi + \hat{L}_\chi^2 \right). \quad (50)$$

Thus, the costate evolution from Eq. (34) takes the form given by

$$\begin{aligned} \frac{\partial \hat{\sigma}}{\partial t} &= -i[\hat{H}_\chi, \hat{\sigma}] + \frac{1}{4\tau} \left([\Delta\hat{V}_\chi, \hat{\sigma}]_+ - 2\langle \hat{\sigma} \rangle \hat{V}_\chi \right) \\ &\quad - \frac{r}{2\tau} \left([\Delta\hat{L}_\chi, \hat{\sigma}]_+ - 2\langle \hat{\sigma} \rangle \hat{L}_\chi \right) \\ &\quad + \frac{1}{2\tau} (-2r\hat{L}_\chi + \hat{L}_\chi^2), \end{aligned} \quad (51)$$

which is the same as Eqs. (A8) and (A9). Since Eq. (40) is trace-preserving, we can redefine $\hat{\sigma} = \hat{\sigma} + (1 - \langle \hat{\sigma} \rangle)\hat{\mathbb{1}}$ without changing the value of the stochastic Hamiltonian in Eq. (48). With this redefinition, the evolution of the costate becomes

$$\begin{aligned} \frac{\partial \hat{\sigma}}{\partial t} &= -\hat{\mathfrak{F}}_{\hat{\rho}}^\dagger(\hat{\sigma}, r) \\ &= -i[\hat{H}_\chi, \hat{\sigma}] + \frac{1}{4\tau} [\Delta\hat{V}_\chi, \hat{\sigma}]_+ - \frac{r}{2\tau} [\Delta\hat{L}_\chi, \hat{\sigma}]_+. \end{aligned} \quad (52)$$

Note that this simplification might not be possible for a different cost function f^0 . Now, the CDJP stochastic Hamiltonian in Eq. (48) becomes

$$\begin{aligned} \mathcal{H}(\hat{\sigma}, \hat{\rho}, r, \chi) &= \left\langle i[\hat{H}_\chi, \hat{\sigma}] - \frac{1}{4\tau} [\Delta\hat{V}_\chi, \hat{\sigma}]_+ \right\rangle \\ &\quad - \frac{1}{2\tau} (r - r_\chi)^2 + \frac{1}{2\tau} r_\chi^2, \end{aligned} \quad (53)$$

with

$$r_\chi = \langle \hat{L}_\chi \rangle + \frac{1}{2} \left\langle [\Delta\hat{L}_\chi, \hat{\sigma}]_+ \right\rangle. \quad (54)$$

For the most likely readout, according to the Pontryagin's maximum principle, the Hamiltonian achieves supremum

for given $\hat{\sigma}, \hat{\rho}$ and χ . Thus, $r = r_\chi$ is the most likely readout. The optimal Hamiltonian is

$$\mathcal{H}^*(\hat{\sigma}, \hat{\rho}, \chi) = \left\langle i[\hat{H}_\chi, \hat{\sigma}] - \frac{1}{4\tau} [\Delta\hat{V}_\chi, \hat{\sigma}]_+ \right\rangle + \frac{1}{2\tau} r_\chi^2, \quad (55)$$

which achieves supremum for the optimal control χ , for given $\hat{\sigma}$ and $\hat{\rho}$. Note that the form of the above Hamiltonian is the same as Eq. (15), as expected.

Thus, we see that when the cost function is the CDJ action, the Pontryagin's maximum principle gives the most likely path equations.

B. Optimal control for a monitored harmonic oscillator

We apply the preceding formalism to find optimal control protocols for a monitored harmonic oscillator. First, we introduce a parametric control to the harmonic oscillator Hamiltonian

$$\hat{H} = \frac{1}{2} (\hat{X}^2 + \hat{P}^2) + \lambda_1(t)\hat{X}^2, \quad (56)$$

where $\lambda_1(t)$ is a control parameter with its value bounded by λ_1^{\max} . The additional \hat{X}^2 term can represent oscillators with tunable frequencies. Such parametric Hamiltonians have been previously considered for cooling [61, 62]. The oscillator is undergoing adaptive quadrature measurements expressed by the observable \hat{L}_θ in Eq. (17). We look at all the trajectories starting from a specific initial state $\hat{\rho}(t=0) = \hat{\rho}_i$ and reaching some specified final state $\hat{\rho}(t=t_f) = \hat{\rho}_f$. We ask, what choice of the controls λ_1 and θ , as functions of time, will maximize the readout probabilities? In other words, we look for the trajectory with the highest probability under the allowed control values.

The conditional state evolution along the most likely path is expressed by Eq. (21a), with the Hamiltonian given by Eq. (56). To look at the most likely readout evolution, we define the following scalars (see appendix E)

$$\begin{aligned} \Gamma(n, m) &= \text{Tr} \left(\hat{X}^n \hat{P}^m \hat{\Omega} \right), \\ \kappa(n, m) &= i \text{Tr} \left(\hat{X}^n \hat{P}^m \hat{\Lambda} \right), \end{aligned} \quad (57)$$

with $\hat{\Omega} = \frac{1}{2} [\hat{\rho}, \hat{\sigma}]_+$ and $\hat{\Lambda} = [\hat{\rho}, \hat{\sigma}]$. Then, the optimal readout is

$$r_\theta = \cos \theta \Gamma(1, 0) + \sin \theta \Gamma(0, 1). \quad (58)$$

The evolution of the optimal readout can be found by

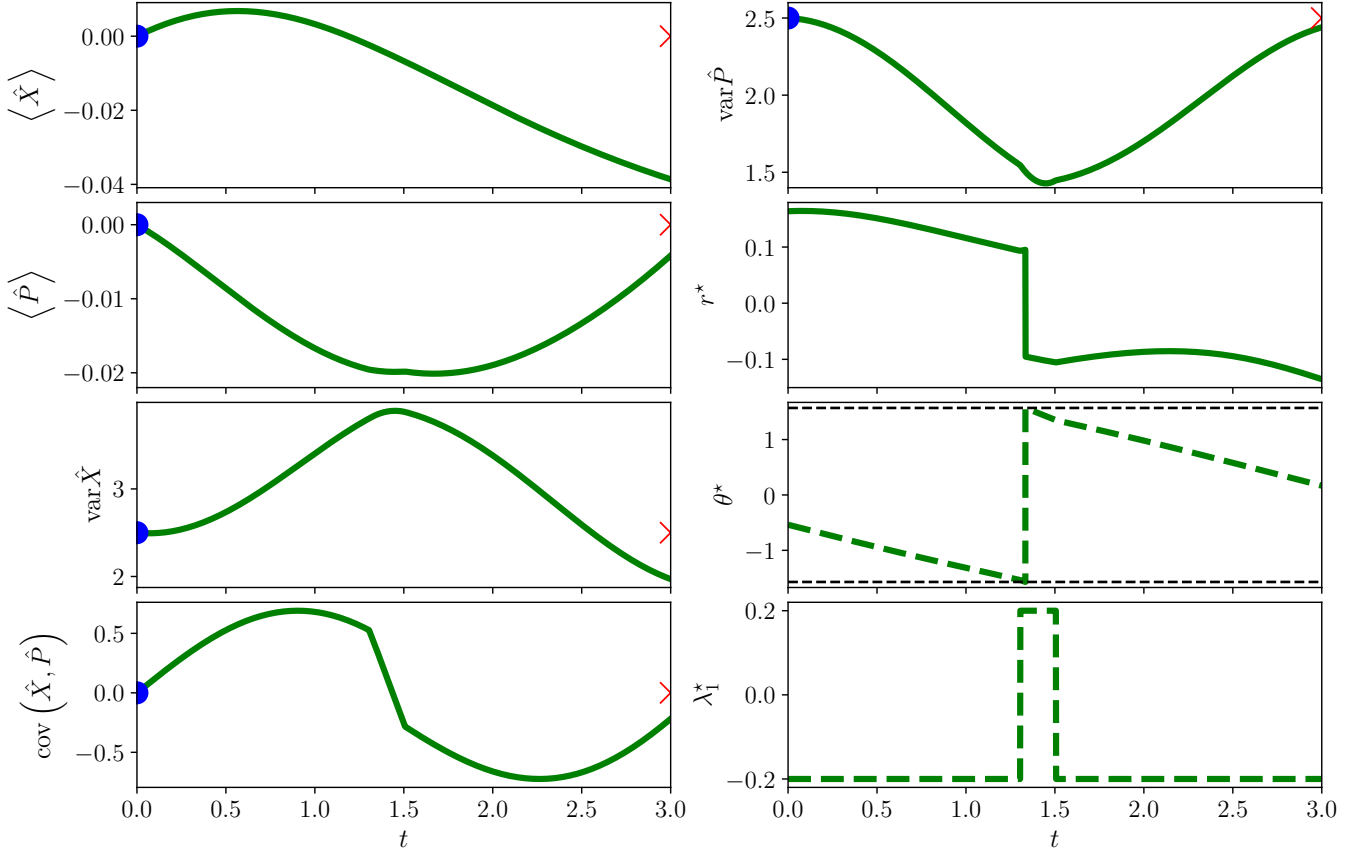


FIG. 3. Optimal control for $|\psi(t=0)\rangle = |\psi_i\rangle = \frac{|0\rangle - |4\rangle}{\sqrt{2}}$ and $|\psi(t=3.0)\rangle = |\psi_f\rangle = \frac{|0\rangle + |4\rangle}{\sqrt{2}}$ with collapse timescale $\tau = 15.0$. Time and the collapse timescale are in the units of the inverse of the oscillator frequency. The left panels from top to bottom show the time evolution of the expectation values of the position and momentum, and the variance of position and covariance of position and momentum, respectively, under optimal control. The top panel on the right-hand side shows the evolution of the momentum variance. All the observables are scaled to be dimensionless (see Sec. II B). The blue dots show the initial state, and the red ‘x’ show the final state. The second panel (from the top) on the right-hand side shows the most likely readout under optimal control. The third and fourth panels on the right-hand side show the optimal control protocols. In other words, they show the optimal measurement quadrature and parametric potential strength. As explained in the text, the potential strength, λ_1^* , is of “bang-bang” form. The final state here is reached with 95.46% fidelity (see appendix F).

integrating the following set of equations

$$\frac{d\Gamma(1,0)}{dt} = \Gamma(0,1) - \frac{\sin\theta}{4\tau} (\cos\theta\kappa(1,0) + \sin\theta\kappa(0,1)), \quad (59a)$$

$$\frac{d\Gamma(0,1)}{dt} = -(1 + 2\lambda_1)\Gamma(1,0) + \frac{\cos\theta}{4\tau} (\cos\theta\kappa(1,0) + \sin\theta\kappa(0,1)), \quad (59b)$$

$$\frac{d\kappa(1,0)}{dt} = \kappa(0,1), \quad \frac{d\kappa(0,1)}{dt} = -(1 + 2\lambda_1)\kappa(1,0). \quad (59c)$$

The optimal Hamiltonian in Eq. (55) can be written as

$$\mathcal{H}^*(\hat{\sigma}, \hat{\rho}, \theta, \lambda_1, \lambda_2) = -i\text{Tr}(\hat{H}\hat{\Lambda}) + \frac{1}{2\tau} \left(\text{Tr}(\hat{L}_\theta\hat{\Omega}) \right)^2 - \frac{1}{2\tau} \text{Tr}(\hat{L}_\theta^2\hat{\Omega}), \quad (60)$$

which can be expressed in terms of the Eqs. (57) as

$$\mathcal{H}^* = -\left(\frac{1}{2}(1 + 2\lambda_1)\kappa(2,0) + \frac{1}{2}\kappa(0,2) \right) + \frac{1}{4\tau} \left(\Gamma(1,0)^2 + \Gamma(0,1)^2 - \Gamma(2,0) - \Gamma(0,2) \right) + \frac{1}{2\tau} \left(A_\Gamma \cos 2\theta + B_\Gamma \sin 2\theta \right), \quad (61)$$

where

$$\begin{aligned} A_\Gamma &= \frac{1}{2} \left(\Gamma(1,0)^2 - \Gamma(0,1)^2 - \Gamma(2,0) + \Gamma(0,2) \right) \\ B_\Gamma &= \Gamma(1,0)\Gamma(0,1) - \tilde{\Gamma}(1,1). \end{aligned} \quad (62)$$

We define $\tilde{\Gamma}(1,1) = \Gamma(1,1) - \frac{i}{2}$ such that B_Γ is real. Then, according to condition I of the Pontryagin's maximum principle, the optimal value of λ_1 is given by

$$\lambda_1^*(t) = -\lambda_1^{\max} \text{sign}(\kappa(2,0)). \quad (63)$$

Thus, the Pontryagin maximum principle analytically shows that the optimal parametric potential should have a bang-bang form. Similarly, we define $A_\Gamma = R_\Gamma \cos \phi_\Gamma$ and $B_\Gamma = R_\Gamma \sin \phi_\Gamma$ such that $R_\Gamma = \sqrt{A_\Gamma^2 + B_\Gamma^2} \geq 0$. Then the final term in Eq. (61) can be written as $\frac{R_\Gamma}{2\tau} \cos(\phi_\Gamma - 2\theta)$, which should take its maximum value for optimal θ . Assuming $\phi_\Gamma \in [-\pi, \pi]$ and $\theta \in [-\frac{\pi}{2}, \frac{\pi}{2}]$ (since replacing \hat{L}_θ by $-\hat{L}_\theta$ does not change the optimal paths), the optimal θ is given by

$$\theta^*(t) = \frac{\phi_\Gamma}{2}. \quad (64)$$

For optimal control, the value of the optimal Hamiltonian is given by

$$\begin{aligned} \mathcal{H}^* &= \lambda_1^{\max} |\kappa(2,0)| - \frac{1}{2} \left(\kappa(2,0) + \kappa(0,2) \right) + \frac{1}{2\tau} R_\Gamma \\ &+ \frac{1}{4\tau} \left(\Gamma(1,0)^2 + \Gamma(0,1)^2 - \Gamma(2,0) - \Gamma(0,2) \right). \end{aligned} \quad (65)$$

The evolutions of the second order Γ terms are given by

$$\begin{aligned} \frac{d\Gamma(2,0)}{dt} &= 2\tilde{\Gamma}(1,1) + \frac{\sin \theta}{2\tau} \left(r_\theta \kappa(1,0) \right. \\ &\left. - \cos \theta \kappa(2,0) - \sin \theta \kappa(1,1) \right), \end{aligned} \quad (66a)$$

$$\begin{aligned} \frac{d\tilde{\Gamma}(1,1)}{dt} &= - (1 + 2\lambda_1) \Gamma(2,0) + \Gamma(0,2) \\ &+ \frac{1}{4\tau} \left(r_\theta \left(\sin \theta \kappa(0,1) - \cos \theta \kappa(1,0) \right) \right. \\ &\left. + \left(\cos^2 \theta \kappa(2,0) - \sin^2 \theta \kappa(0,2) \right) \right), \end{aligned} \quad (66b)$$

$$\begin{aligned} \frac{d\Gamma(0,2)}{dt} &= - 2(1 + 2\lambda_1) \tilde{\Gamma}(1,1) + \frac{\cos \theta}{2\tau} \left(- r_\theta \kappa(0,1) \right. \\ &\left. + \left(\sin \theta \kappa(0,2) + \cos \theta \kappa(1,1) \right) \right). \end{aligned} \quad (66c)$$

Similarly, the second order κ evolutions are given by.

$$\begin{aligned} \frac{d\kappa(2,0)}{dt} &= 2\kappa(1,1) + \frac{2 \sin \theta}{\tau} \left(- r_\theta \Gamma(1,0) + \right. \\ &\left. \cos \theta \Gamma(2,0) + \sin \theta \tilde{\Gamma}(1,1) \right), \end{aligned} \quad (67a)$$

$$\begin{aligned} \frac{d\kappa(1,1)}{dt} &= - (1 + 2\lambda_1) \kappa(2,0) + \kappa(0,2) \\ &+ \frac{1}{\tau} \left(r_\theta \left(\cos \theta \Gamma(1,0) - \sin \theta \Gamma(0,1) \right) \right. \\ &\left. + \left(- \cos^2 \theta \Gamma(2,0) + \sin^2 \theta \Gamma(0,2) \right) \right), \end{aligned} \quad (67b)$$

$$\begin{aligned} \frac{d\kappa(0,2)}{dt} &= - 2(1 + 2\lambda_1) \kappa(1,1) + \frac{2 \cos \theta}{\tau} \left(r_\theta \Gamma(0,1) \right. \\ &\left. - \left(\sin \theta \Gamma(0,2) + \cos \theta \tilde{\Gamma}(1,1) \right) \right). \end{aligned} \quad (67c)$$

Note that the equations (59), (66) and (67) are self-contained. Thus, the optimal controls can be found by integrating Eq. (21a) along with Eqs. (59), (66), and (67) with the control values given by Eqs. (63) and (64). Instead of integrating the costate $\hat{\sigma}$, which has the same dimension as $\hat{\rho}$, we just need to integrate ten scalars $\Gamma(1,0)$, $\Gamma(0,1)$, $\kappa(1,0)$, $\kappa(0,1)$, $\Gamma(2,0)$, $\tilde{\Gamma}(1,1)$, $\Gamma(0,2)$, $\kappa(2,0)$, $\kappa(1,1)$, $\kappa(0,2)$.

Pontryagin maximum principle provides a necessary condition on the optimality of the protocol. Thus, after solving equations (59), (66) and (67) with optimal controls Eqs. (63) and (64), we need to ensure the cost function (45) obtains the minimum possible value. Exploring the control protocols for state preparation that guarantee a unique solution will be a worthwhile endeavor in the future.

C. Example 1: Preparation of a Binomial Code Word

Now, we apply our general results to problems in Bosonic quantum computing. In the subsequent analysis, the final time is $t_f = 3.0$ and the collapse time scale $\tau = 15.0$, both in units of the harmonic oscillator frequency. The quadratures and the readouts are made dimensionless (see Sec. II B).

We consider the evolution from the initial state $|\psi(t=0)\rangle = |\psi_i\rangle = \frac{|0\rangle - |4\rangle}{\sqrt{2}}$ to the final state $|\psi(t=3.0)\rangle = |\psi_f\rangle = \frac{|0\rangle + |4\rangle}{\sqrt{2}}$ with measurement collapse timescale $\tau = 15.0$ and $\lambda_1^{\max} = 0.2$. The final state represents a logical state of a binomial code that can protect

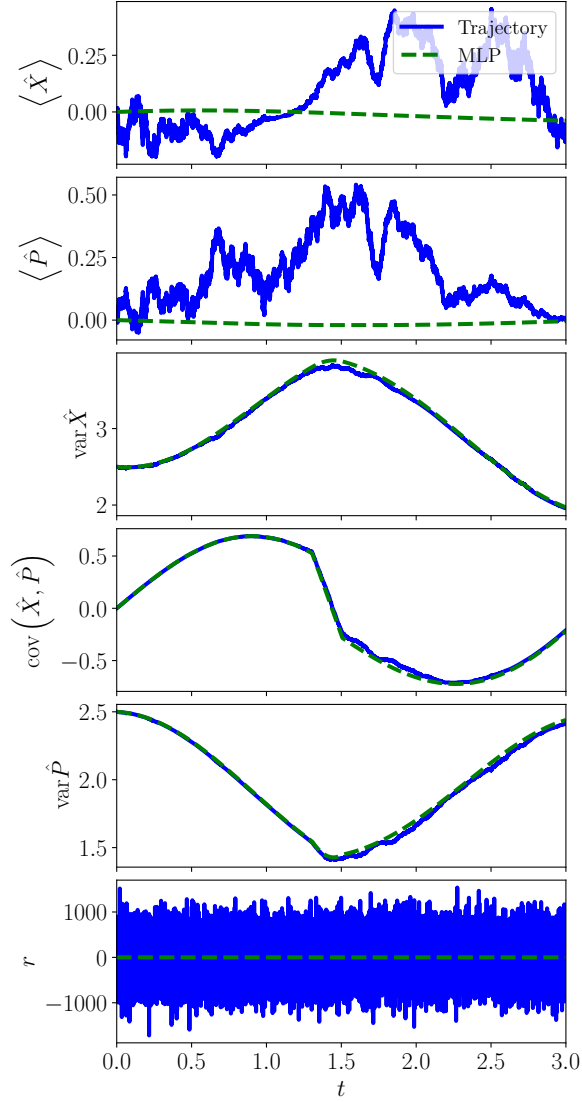


FIG. 4. From top to bottom, the panels show the time evolution of the expectation value of the position, the expectation value of momentum, the variance of position, the covariance of position and momentum, the variance of momentum, and the readout under the control in Fig. 3. The green dashed line shows the most likely path under optimal control shown in Fig. 3. All the observables are scaled to be dimensionless (see Sec. II B). The blue curve shows a sample simulated stochastic trajectory under the optimal control shown in the bottom two right panels of Fig. 3, starting from the initial state $|\psi_i\rangle = \frac{|0\rangle - |4\rangle}{\sqrt{2}}$. The collapse timescale is $\tau = 15.0$ (time and the collapse timescale are in the units of the inverse of the oscillator frequency). The quadratures and the readout are dimensionless (see Sec. II B). We see that the expectation values along the trajectory jitter around the most likely path. Additionally, the trajectory closely follows the evolution of the variances and the covariance. The expectation values for the most likely path and the optimal readout appear flat because the corresponding scales involved with the stochastic trajectory are much larger (see appendix G for the numerical method adopted to simulate trajectories).

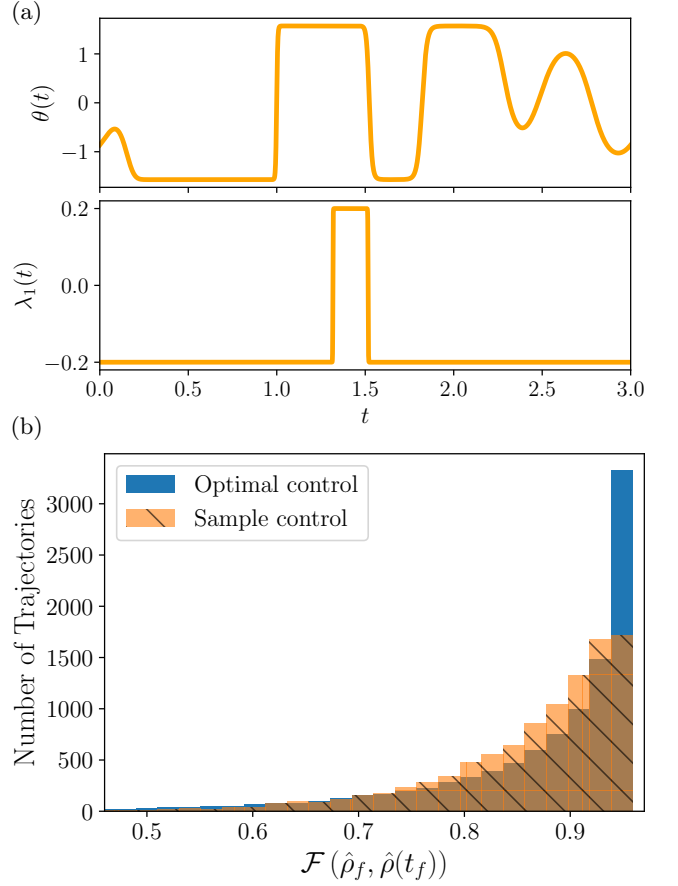


FIG. 5. In panel (a), the top (bottom) plot shows sample measurement quadrature (parametric potential strength) as a function of time for collapse timescales $\tau = 15.0$ (in units of $1/\text{oscillator frequency}$) for such that trajectories starting from $|\psi_i\rangle = \frac{|0\rangle - |4\rangle}{\sqrt{2}}$ have a significant probability of reaching $|\psi_f\rangle = \frac{|0\rangle + |4\rangle}{\sqrt{2}}$ at $t = 3.0$. Note, $\lambda_1(t)$ has a structure almost identical to $\lambda_1^*(t)$ shown in Fig. 3. However, $\theta(t)$ here is very different from $\theta^*(t)$. Panel (b) shows the histogram of final state fidelities (with respect to the target state $|\psi_f\rangle = \frac{|0\rangle + |4\rangle}{\sqrt{2}}$) of 10,000 simulated trajectories under the optimal control in Fig. 3 (blue, vertical hatched) and the sample control presented in panel (a) (orange, diagonal hatched). We see that a significantly higher number of trajectories can achieve very high fidelities under optimal control.

against a single photon loss³. The initial state corresponds to an error word under no jump evolution [2, 59]. We wish to solve for the adaptive quadrature measurement and parametric Hamiltonian control that minimizes Eq. (45) amongst the trajectories starting from $|\psi_i\rangle$ and reaching $|\psi_f\rangle$. The results of the optimization are shown in Fig. 3. Here, the final state is reached with 95.46% fidelity (see numerical methods in appendix F). The figure

³ The other logical state being $|2\rangle$.

shows the most likely path under optimal control in the four left and topmost right panels. The second panel on the right-hand side shows the most likely readout under optimal control. The optimal measurement quadrature and parametric potential strengths are shown in the bottom two panels on the right. As per Eq. (63), the optimal parametric potential is of the “bang-bang” form with two sign switches close to $t = 1.5$. The optimal quadrature shows a saw-tooth-like evolution with a discontinuity near $t = 1.4$.

In Fig. 4, we compare the evolutions of a sample stochastic trajectory (blue solid) and the most likely path (green dashed) under optimal control. We see that the trajectory follows the most likely path very closely.

It is insightful to compare the statistics of the trajectories under the optimal control with those under a sample control. In other words, we are interested in generating a control $\theta(t)$ and $\lambda_1(t)$ such that trajectories starting from $|\psi_i\rangle$ at $t = 0$ have a non-infinitesimal probability of reaching $|\psi_f\rangle$ at $t = 3.0$. Fig. 5(a) provides one such example (see appendix H for the relevant numerical methods). Here, the final state can be reached with 95.58% fidelity. Fig. 5(b) shows the histograms of the final state fidelities (with respect to the target state) for trajectories under optimal control and those under the sample control. Under the optimal control, 57.08% (18.31%) of trajectories have fidelities of more than 90% (95%). With the sample control, 46.01% (6.19%) of the trajectories have a fidelity of more than 90% (95%). This is around a 24% (196%) increase in the number of trajectories reaching 90% (95%) fidelities. Although the optimal control was computed with fixed end points assumption, Fig. 5(b) shows that control derived in this manner can still be useful for state preparation. We note that the histogram does not constitute a formal proof of the optimality of the protocol. To ensure optimality, we must restrict ourselves to trajectories between $|\psi_i\rangle$ and $|\psi_f\rangle$ and consider all possible controls. The proof of the optimality of a specific protocol is beyond the scope of this article.

D. Example 2: Parametric cooling from a cat state

Two-component Schrödinger’s cat states constitute an important family of non-Gaussian harmonic oscillator states. Such states are coherent superpositions of coherent states [60, 124]. They can be generated by two-photon-driven dissipative processes and provide a Bosonic encoding that can protect against dephasing errors [125]. For our second example, we consider the even cat state $|\psi(t=0)\rangle = |\psi_i\rangle \propto |\alpha\rangle + |-\alpha\rangle$ with $\alpha = 0.25 - i0.75$ as the initial state. The final state is the ground state $|\psi(t=3.0)\rangle = |0\rangle$ with collapse timescale⁴

$\tau = 15.0$ and $\lambda_1^{\max} = 0.2$. In other words, we are looking at parametric cooling starting from the initial state $|\psi_i\rangle$ [61, 62]. The final state should be free to consider the full generality of parametric cooling. For simplicity, we limit our analysis to fixed-endpoint scenarios. We will see shortly that optimal control computed under such restriction can still be very useful. Fig. 6 shows the optimal control protocol for the problem. In this case, our simulations achieved a final state fidelity of 97.49%. The parametric potential strength is of “bang-bang” form and changes sign twice. The optimal quadrature has a discontinuity near $t = 1.7$.

Fig. 7 (a) shows a sample control (reaching final state with 98.21% fidelity) with a trajectory starting from $|\psi_i\rangle$ and reaching $|\psi_f\rangle$ at $t = 3.0$. Note, the λ_1 is almost identical to the optimal λ_1^{opt} shown in Fig. 6. Fig. 7 (b) compares the histograms of the final state fidelities for 10,000 simulated stochastic trajectories under the sample and the optimal control. Under the optimal control, 97.00% (79.51%) of the trajectories have fidelities of more than 90% (95%). With the sample control, 84.31% (56.73%) of the trajectories have a fidelity of more than 90% (95%). This is around a 15% (39%) increase in the number of trajectories reaching 90% (95%) fidelities. Therefore, we again see a significant increase in the probability of high-fidelity state preparation under optimal control.

E. Example 3: Cat state to cat state

We now consider a cat state to cat state evolution. $|\psi(t=0)\rangle = |\psi_i\rangle \sim |\alpha_i\rangle + |-\alpha_i\rangle$ and $|\psi(t=3.0)\rangle = |\psi_f\rangle \sim |\alpha_f\rangle + |-\alpha_f\rangle$ with $\alpha_i = -0.25 + 1.55i$ and $\alpha_f = 1.35 - 0.75i$. The collapse timescale is $\tau = 15.0$ (in units of $1/\text{oscillator frequency}$). The optimal control is shown in Fig. 8. The final state is reached with 95.59% fidelity. In this example, λ_1^\dagger has two jumps between $0.5 < t < 1.0$. The optimal quadrature has a sawtooth behavior with a discontinuity around $t \sim 2.1$.

In Fig. 9(a), we show a sample control that can reach 97.94% fidelity. In Fig. 9 (b), we compare the histograms of 10,000 trajectories simulated under the optimal control and the sample control. Applying the optimal control leads to more trajectories reaching close to the target state. Under the optimal control, 92.68% (47.17%) of trajectories have fidelities of more than 90% (95%). With the sample control, 32.78% (18.89%) of the trajectories have a fidelity of more than 90% (95%). This is around a 182% (150%) increase in the number of trajectories reaching 90% (95%) fidelities. Again, we see a superior performance of the optimal control. In this example, we have limited the cat state sizes to $|\alpha|^2 \sim 2.4$ due to simulation constraints. The generation of larger cat states and cooling from them in the presence of a non-linear parametric potential (see appendix E) are interesting future avenues for exploration.

These three examples demonstrate the benefits of employing most likely path-based optimal control protocols

⁴ Again, time and the collapse timescale τ are in units of $1/\text{oscillator frequency}$.

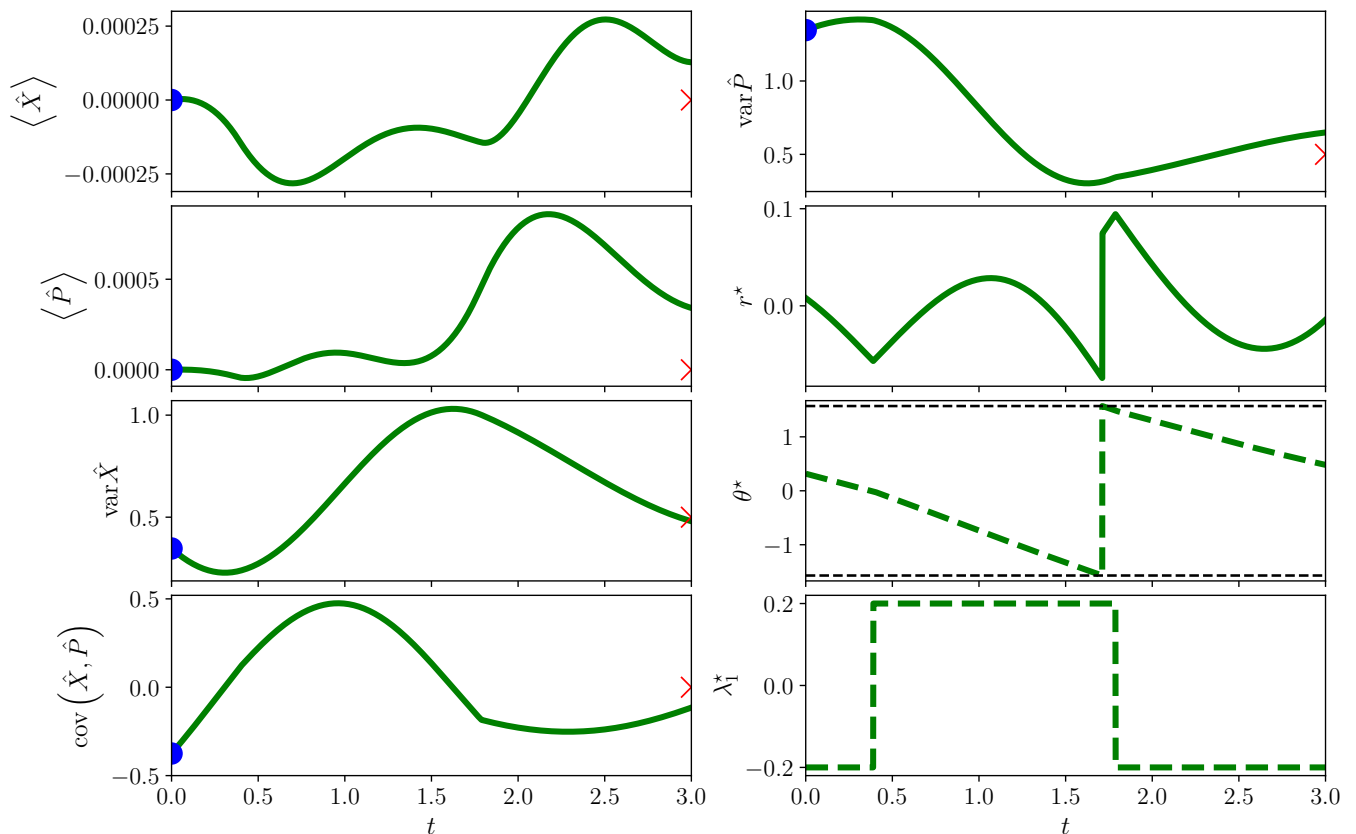


FIG. 6. Optimal control for $|\psi(t=0)\rangle \propto |\alpha\rangle + |-\alpha\rangle$ with $\alpha = 0.25 - i0.75$ and $|\psi(t=3.0)\rangle = |\psi_f\rangle = |0\rangle$. The collapse timescale is $\tau = 15.0$ (in units of $1/\text{oscillator frequency}$). Again, the left panels from top to bottom show the time evolution of the expectation values of the position and momentum, and the variance of position and covariance of position and momentum, respectively, under optimal control. The top panel on the right-hand side shows the evolution of the momentum variance. The blue dots show the initial state, and the red ‘x’ show the final state. The second panel (from the top) on the right-hand side shows the most likely readout under optimal control. The third and fourth panels on the right-hand side show the optimal quadrature θ^* and parametric potential strength λ_1^* . Again, we see a “bang-bang” form for λ_1^* with value $\lambda_1 = 0.2$ approximately between $0.4 < t < 1.8$. θ^* has a discontinuity near $t \approx 1.7$. The final state here is reached with 97.49% fidelity.

for continuously monitored systems.

IV. DISCUSSION

In this work, we have formulated a costate-based description of the Chantasri-Dressel-Jordan most likely path formalism for general continuously monitored systems. We show that the system’s evolution along the most likely path can be expressed in terms of coupled evolution equations of the system’s state and a costate operator. Next, we provide a general Pontryagin maximum principle formulation for the optimal control of a quantum system undergoing arbitrary evolution. The cost function is assumed to be general. For general nonlinear evolution, the costate evolution might differ from the negative adjoint evolution prevalent in the literature [65, 66]. Such differences can be crucial for a continuously monitored system since the conditional dynamics is nonlinear in this case. We derive the CDJ most likely

paths as a special case of the general Pontryagin principle when the cost function corresponds to the probability density of the readouts. The costate evolution can be reduced to the negative adjoint of the state evolution under an operator transformation.

We look at a continuously monitored harmonic oscillator with a parametric control potential and undergoing variable quadrature measurements. In this case, the costate evolution can be substituted for 10 scalar parameter evolutions. Such dimensionality reduction leads to fast numerical simulations. The Pontryagin’s maximum principle lets us derive the analytical forms of the optimal parametric potential strength and the optimal measurement quadrature. The former is of “bang-bang” form. We look at three fixed-endpoint problems. In the first one, we look at the preparation of binomial code word $\frac{|0\rangle+|4\rangle}{\sqrt{2}}$ starting from $\frac{|0\rangle-|4\rangle}{\sqrt{2}}$. The second example looks at cooling to the ground state starting from an even cat state. In the third example, we look at a cat state to cat state

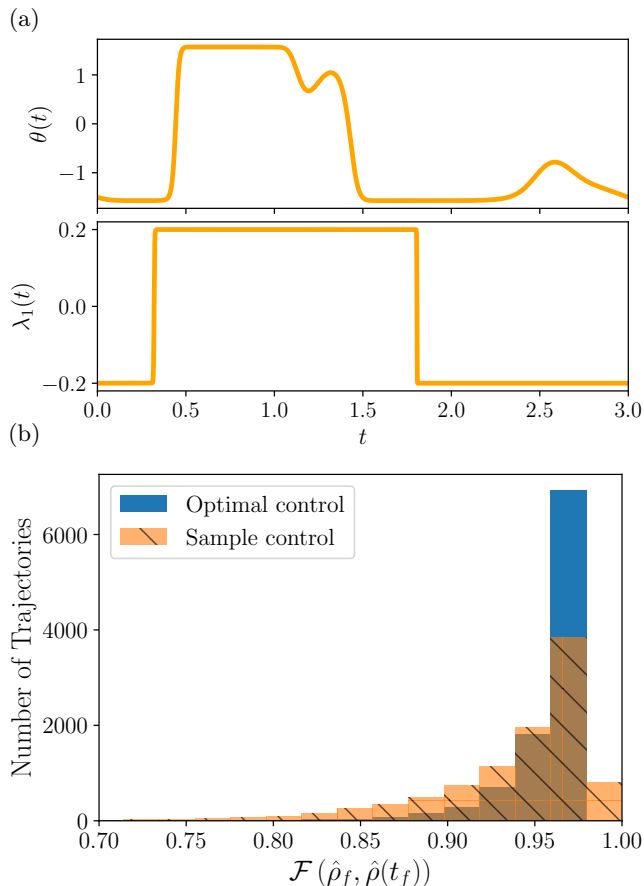


FIG. 7. In panel (a), the top (bottom) plot shows sample measurement quadrature (parametric potential strength) as a function of time such that trajectories starting from $|\psi_i\rangle \propto |\alpha\rangle + |-\alpha\rangle$ with $\alpha = 0.25 - i0.75$ have a significant probability of reaching $|\psi_f\rangle = |0\rangle$ at $t = 3.0$ with $\tau = 15.0$. Time and collapse timescales are in units of the inverse of the oscillator frequency. Again, $\lambda_1(t)$ has a structure very similar to the $\lambda_1^*(t)$ shown in Fig. 6. $\theta(t)$ here is very different from $\theta^*(t)$. Panel (b) shows the histogram of final state fidelities (with respect to the target state $|\psi_f\rangle = |0\rangle$) of 10,000 simulated trajectories under the optimal control in Fig. 6 (blue, vertical hatched) and the sample control presented in panel (a) (orange, diagonal hatched). A significantly higher number of trajectories can reach large fidelities than trajectories under the sample control. We see a small number of trajectories reach very close to fidelity 1.0 under the sample control. This is because the numerical simulation for finding the sample control can achieve better convergence to the target state in this case (see appendices H and F).

evolution. For all three examples, we compare the performance of simulated trajectories under the optimal control and a sample control. We see trajectories under the optimal control perform significantly better compared to the trajectories under the sample control. Compared to the latter case, under optimal control, a significantly larger number of trajectories can reach high fidelities with respect to the target state. The results demonstrate that

even under the fixed-endpoint assumption, optimal control found from the CDJ-Pontryagin approach can be very useful for state preparation in continuously monitored systems.

The \hat{X}^2 parametric potential and the quadrature measurements offer limited flexibility for state preparation in continuous variable systems. For universal quantum computation, anharmonic potential should be included [120, 126]. The limitation of a quadratic potential can be seen in our optimal control computations. In simulations, we find the initial values of $\Gamma(n, m)$ and $\kappa(n, m)$ such that their evolution according to Eqs. (59), (66), (67), (63) and (64) can bring the final state as close as possible to the target state. Our simulations converge around 95-97% fidelities, while solutions with more than 99% fidelities would be ideal. Introducing cubic or higher order potential might lead to better final state fidelities. Also, note that condition I, presented in sec. III, is a necessary condition, not a sufficient one. In our simulations, we observe multiple possible solutions for the equations presented in sec. III B. Additional tests are needed to ascertain whether the solution found through Pontryagin's maximum principle is truly optimal. Our numerical scheme ensures (see appendix F) that the cost Eq. (45) associated with the optimal control is as small as possible. As the final state fidelity reaches 90-95%, subsequent iterations of the numerical optimization update the candidate solution only if the cost in Eq. (45) is reduced. This leads to a Pareto front optimization between final state fidelity and readout probabilities. Robust numerical methods that guarantee high-fidelity optimal solutions should be investigated in the future. We refer the formal proof of the optimality of the solutions we found to future explorations.

On a related note, we have previously proven the existence of a unique optimal path for Gaussian state quantum harmonic oscillators [54]. The situation might be different for other continuously monitored systems. It is known that monitored qubits might show multiple optimal paths [47, 48, 52]. It is worth exploring whether multiple optimal paths can arise for monitored oscillators in non-Gaussian states. Also, in certain scenarios, optimal paths or an optimal control protocol might not exist. These issues connect broadly to the question of controllability. A thorough exploration of the existence and uniqueness of the optimal paths and the optimal control protocols is needed.

Our work can be useful for finding optimal control for state preparation [127, 128], dissipative stabilization [6, 56, 58], feedback cooling [63, 64, 129], etc. Implementing our framework for finding optimal controls for continuous error correction of Bosonic codes is a natural next step [41, 59, 120, 130, 131]. A similar approach can be adopted for autonomous quantum error correction [13, 132–134].

In our work, we adopted the readout probabilities in a continuous measurement as the cost function. Other cost functions, such as the expectation value of the Hamiltonian, might be useful for running quantum algorithms

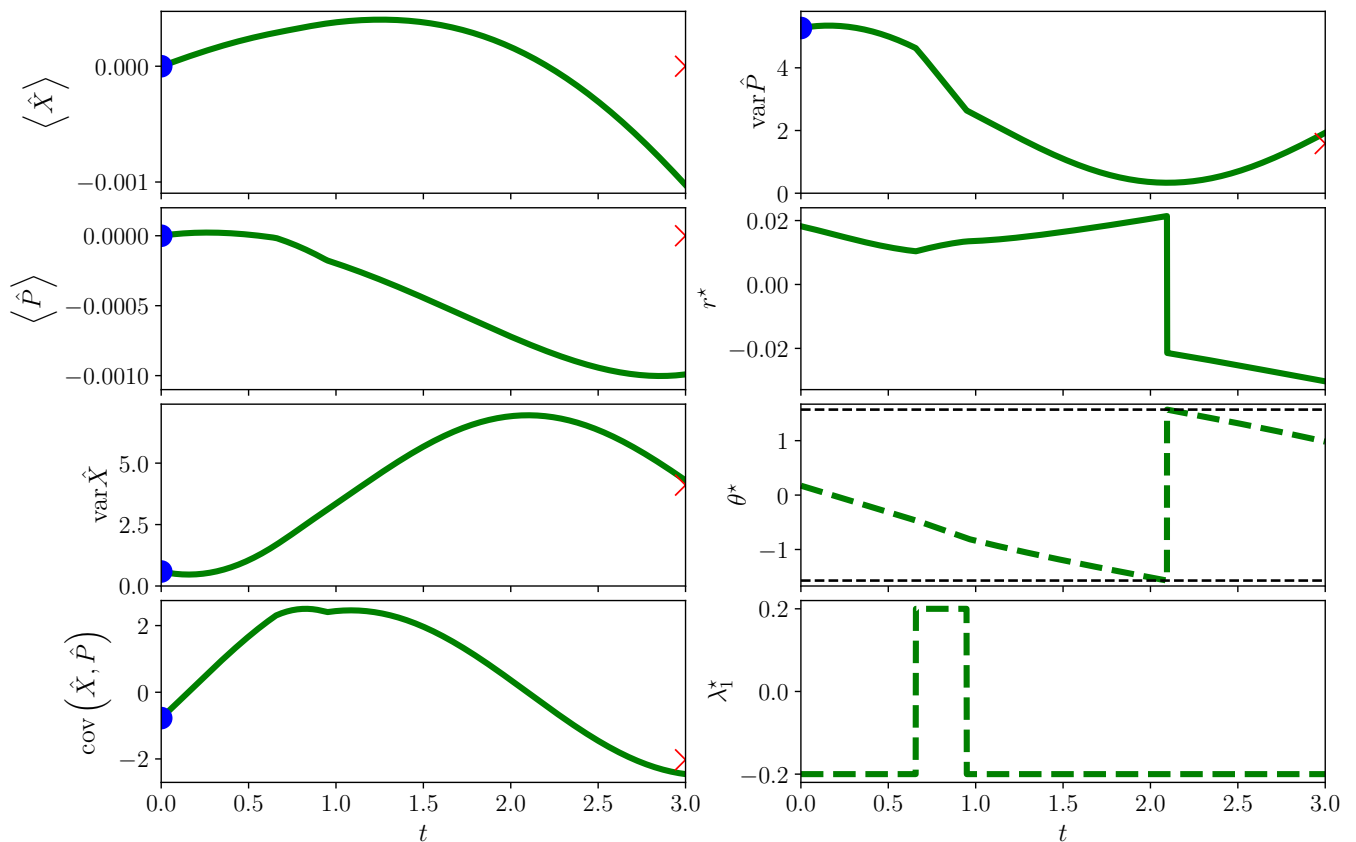


FIG. 8. We consider now cat state to cat state evolution. $|\psi(t=0)\rangle = |\psi_i\rangle \sim |\alpha_i\rangle + |-\alpha_i\rangle$ and $|\psi(t=3.0)\rangle = |\psi_f\rangle \sim |\alpha_f\rangle + |-\alpha_f\rangle$ with $\alpha_i = -0.25 + 1.55i$ and $\alpha_f = 1.35 - 0.75i$, and the measurement collapse timescale $\tau = 15.0$. Time and collapse timescales are in units of the inverse of the oscillator frequency. The left panels from top to bottom show the time evolution of the expectation values of the position and momentum, and the variance of position and covariance of position and momentum, respectively, under optimal control. The top panel on the right-hand side shows the evolution of the momentum variance. The blue dots show the initial state and the red ‘x’ show the final state. Our numerical method converges to a fidelity of 95.59%. The second panel (from the top) on the right-hand side shows the most likely readout under optimal control. The third and fourth panels on the right-hand side show the optimal quadrature θ^* and parametric potential strength λ_1^* . θ^* has a sawtooth-like behavior with a discontinuity near $t = 2.1$. λ_1^* has a “bang-bang” form with two discontinuities between $0.5 < t < 1.0$.

[69, 135] or solving classical problems [4, 73]. One can adopt the entanglement of formation as a cost function to prepare entangled states [29, 50, 53, 136, 137]. With our framework, quantum optimal control for many body systems can be studied. One example is a dissipative Bosonic Kitaev chain in the presence of quadratic bosonic Lindbladians [138, 139]. For this system, a Gaussian state restriction might be analytically and numerically tractable [140].

Solving for most likely paths or optimal control can be hard, even numerically. By introducing the costate, the dimensionality of the problem increases twofold. The model reduction strategy we have presented is helpful for a monitored oscillator with quadratic control Hamiltonian. In this case, we keep track of 10 additional scalars that depend on the commutator and anti-commutator of the state and the costate. It will be worthwhile to explore other model reduction strategies for finding optimal control. On this note, neural network-based methods have

been adopted to optimize state preparation schemes [141] and feedback control protocols [142–145].

Finally, the conditional stochastic evolution considered here is Markovian. Markovian approximation is valid when detector correlation timescales are much smaller than the time scales we are interested in. In such a situation, the memory effects of the system-detector interaction are negligible. It will be insightful to explore the CDJ-Pontryagin formalism for non-Markovian dynamics. A pseudo-Lindbladian master equation-based description can be helpful in this scenario [65, 146, 147]. In conclusion, our work provides a systematic way of finding optimal control for systems undergoing general nonlinear dynamics and offers several possible avenues for further exploration.

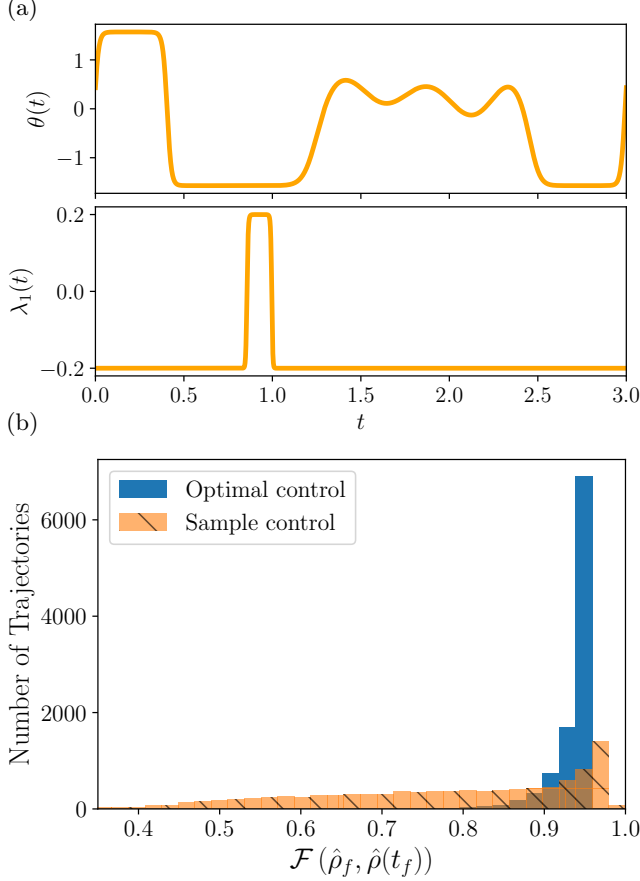


FIG. 9. We consider now cat state to cat state evolution. $|\psi(t=0)\rangle = |\psi_i\rangle \sim |\alpha_i\rangle + |-\alpha_i\rangle$ and $|\psi(t=3.0)\rangle = |\psi_f\rangle \sim |\alpha_f\rangle + |-\alpha_f\rangle$ with $\alpha_i = -0.25 + 1.55i$ and $\alpha_f = 1.35 - 0.75i$ with $\tau = 15.0$. Time and collapse timescales are in units of the inverse of the oscillator frequency. Panel (a) shows a sample control that can reach a fidelity of 97.94%. The parametric potential is similar to the one shown in Fig. 8, although the region with $\lambda_1 = 0.2$ is much thinner. θ_1 is completely different from the optimal quadrature θ_1^* shown in Fig. 8. Panel (b) shows the histogram of the fidelities of 10,000 trajectories at $t = 3.0$ with respect to the target state under optimal control (blue, vertical hatched) and the sample control (orange, diagonal hatched). The optimal control leads to very high fidelities with significantly higher probabilities.

ACKNOWLEDGEMENT

We thank Philippe Lewalle, Adithi Ajith, K. Birgitta Whaley, Alain Sarlette, Yipei Zhang, Sreenath Manikandan, Ryotatsu Yanagimoto, Bibek Bhandari, Alok Nath Singh, Tryphon T. Georgiou, Olga Movilla for helpful discussions. We acknowledge support from the John Templeton Foundation Grant ID 63209 and the Army Research Office grant W911NF-22-1-0258.

Appendix A: Variation of the stochastic action

In this appendix, we look at the variational extremization of the action given by Eqs. (10) and (11). The stochastic action is given by Eqs. (10) and (11). We consider trajectories with initial state $\hat{\rho}_i$ at $t = 0$ and final state $\hat{\rho}_f$ at time $t = t_f$. The variation of the stochastic action due to variations in $\hat{\rho}$, $\hat{\sigma}$, and r is

$$\begin{aligned} \delta\mathcal{S} &= \int_0^{t_f} dt \left(-\text{Tr} \left(\delta\hat{\sigma} \frac{\partial \hat{\rho}}{\partial t} + \hat{\sigma} \frac{\partial \delta \hat{\rho}}{\partial t} \right) + \delta\mathcal{H} \right) \\ &= \int_0^{t_f} dt (\delta\Psi + \delta\mathcal{H}), \end{aligned} \quad (\text{A1})$$

where $\delta\Psi = -\text{Tr} \left(\delta\hat{\sigma} \frac{\partial \hat{\rho}}{\partial t} + \hat{\sigma} \frac{\partial \delta \hat{\rho}}{\partial t} \right)$. Since we look at trajectories with fixed initial and final states $\delta\hat{\rho} = 0$ at the boundaries. Thus, we can write

$$\int_0^{t_f} dt \delta\Psi = \int_0^{t_f} dt \text{Tr} \left(\frac{\partial \hat{\sigma}}{\partial t} \delta \hat{\rho} - \delta \hat{\sigma} \frac{\partial \hat{\rho}}{\partial t} \right). \quad (\text{A2})$$

Variation of the stochastic Hamiltonian

$$\delta\mathcal{H} = \delta\text{Tr}(\hat{\sigma}\mathfrak{F}(\hat{\rho}, r)) - \frac{1}{2\tau} \delta \left(r^2 - 2r \langle \hat{L} \rangle + \langle \hat{L}^2 \rangle \right). \quad (\text{A3})$$

We can derive the following identities

$$\delta\text{Tr} \left(\hat{\sigma} \left(-i[\hat{H}, \hat{\rho}] \right) \right) = \text{Tr} \left(i[\hat{H}, \hat{\sigma}] \delta \hat{\rho} - i\delta \hat{\sigma} [\hat{H}, \hat{\rho}] \right), \quad (\text{A4a})$$

$$\begin{aligned} \delta\text{Tr} \left(-\hat{\sigma} \frac{1}{4\tau} \left[\hat{L}^2 - \langle \hat{L}^2 \rangle, \hat{\rho} \right]_+ \right) &= \\ \text{Tr} \left(-\delta \hat{\sigma} \frac{1}{4\tau} \left[\hat{L}^2 - \langle \hat{L}^2 \rangle, \hat{\rho} \right]_+ \right) &+ \\ - \frac{1}{4\tau} \left(\left[\hat{L}^2 - \langle \hat{L}^2 \rangle, \hat{\sigma} \right]_+ - 2 \langle \hat{\sigma} \rangle \hat{L}^2 \right) \delta \hat{\rho}, & \end{aligned} \quad (\text{A4b})$$

$$\begin{aligned} \delta\text{Tr} \left(\hat{\sigma} \frac{1}{2\tau} r \left[\hat{L} - \langle \hat{L} \rangle, \hat{\rho} \right]_+ \right) &= \frac{\delta r}{2\tau} \left\langle \left[\hat{L} - \langle \hat{L} \rangle, \hat{\sigma} \right]_+ \right\rangle \\ + \text{Tr} \left(\frac{\delta \hat{\sigma}}{2\tau} r \left[\hat{L} - \langle \hat{L} \rangle, \hat{\rho} \right]_+ \right) &+ \\ + \frac{r}{2\tau} \left(\left[\hat{L} - \langle \hat{L} \rangle, \hat{\sigma} \right]_+ - 2 \langle \hat{\sigma} \rangle \hat{L} \right) \delta \hat{\rho} & \end{aligned} \quad (\text{A4c})$$

$$\begin{aligned} - \frac{1}{2\tau} \delta \left(r^2 - 2r \langle \hat{L} \rangle + \langle \hat{L}^2 \rangle \right) &= - \frac{\delta r}{\tau} (r - \langle \hat{L} \rangle) \\ - \frac{1}{2\tau} \text{Tr} \left((-2r\hat{L} + \hat{L}^2) \delta \hat{\rho} \right). & \end{aligned} \quad (\text{A4d})$$

Using Eqs. (A2) and (A4), we can write the variation of the stochastic action in the following form

$$\begin{aligned} \delta\mathcal{S} &= \int_0^{t_f} dt \left(\frac{\delta r}{\tau} \left(\frac{1}{2} \left\langle \left[\hat{L} - \langle \hat{L} \rangle, \hat{\sigma} \right]_+ \right\rangle - (r - \langle \hat{L} \rangle) \right) \right. \\ &\quad \left. + \text{Tr} \left(\delta\hat{\sigma} \left(\hat{\Gamma}_1 - \frac{\partial \hat{\rho}}{\partial t} \right) + \left(-\hat{\Gamma}_2 + \frac{\partial \hat{\sigma}}{\partial t} \right) \delta\hat{\rho} \right), \right. \end{aligned} \quad (\text{A5})$$

where

$$\begin{aligned} \hat{\Gamma}_1 &= -i[\hat{H}, \hat{\rho}] - \frac{1}{4\tau} [\Delta\hat{V}, \hat{\rho}]_+ + \frac{r}{2\tau} [\Delta\hat{L}, \hat{\rho}]_+, \quad (\text{A6a}) \\ \hat{\Gamma}_2 &= -i[\hat{H}, \hat{\sigma}] + \frac{1}{4\tau} \left([\Delta\hat{V}, \hat{\sigma}]_+ - 2\langle \hat{\sigma} \rangle \hat{V} \right) \\ &\quad - \frac{r}{2\tau} \left([\Delta\hat{L}, \hat{\sigma}]_+ - 2\langle \hat{\sigma} \rangle \hat{L} \right) + \frac{1}{2\tau} (-2r\hat{L} + \hat{L}^2). \end{aligned} \quad (\text{A6b})$$

For most likely paths, $\delta\mathcal{S} = 0$ for arbitrary variations of the state, costate, and readout. Therefore, the optimal readout is given by

$$r^* = \langle \hat{L} \rangle + u = \langle \hat{L} \rangle + \frac{1}{2} \left\langle \left[\Delta\hat{L}, \hat{\sigma} \right]_+ \right\rangle, \quad (\text{A7})$$

where u is the optimal noise. Substituting the value of the optimal readout in Eq. (A6), we get

$$\begin{aligned} \hat{\Gamma}_1^{\text{opt}} &= -i[\hat{H}, \hat{\rho}] - \frac{1}{4\tau} [\Delta\hat{V}, \hat{\rho}]_+ + \frac{r^*}{2\tau} [\Delta\hat{L}, \hat{\rho}]_+, \quad (\text{A8a}) \\ \hat{\Gamma}_2^{\text{opt}} &= -i[\hat{H}, \hat{\sigma}] + \frac{1}{4\tau} \left([\Delta\hat{V}, \hat{\sigma}]_+ - 2(\langle \hat{\sigma} \rangle - 1)\hat{V} \right) \\ &\quad - \frac{r^*}{2\tau} \left([\Delta\hat{L}, \hat{\sigma}]_+ - 2(\langle \hat{\sigma} \rangle - 1)\hat{L} \right). \end{aligned} \quad (\text{A8b})$$

The equations for the optimal paths are

$$\frac{\partial \hat{\rho}}{\partial t} = \hat{\Gamma}_1^{\text{opt}}, \quad \frac{\partial \hat{\sigma}}{\partial t} = \hat{\Gamma}_2^{\text{opt}} \quad (\text{A9})$$

The optimal Hamiltonian $\mathcal{H}^*(\hat{\sigma}, \hat{\rho}) = \mathcal{H}(\hat{\sigma}, \hat{\rho}, r^*)$ is given by

$$\begin{aligned} \mathcal{H}^*(\hat{\sigma}, \hat{\rho}) &= \left\langle i[\hat{H}, \hat{\sigma}] - \frac{1}{4\tau} [\Delta\hat{V}, \hat{\sigma}]_+ \right\rangle + \frac{r^*}{\tau} u \\ &\quad - \frac{1}{2\tau} \left(u^2 + \text{Var}(\hat{L}) \right). \end{aligned} \quad (\text{A10})$$

We can always redefine $\hat{\sigma} \equiv \hat{\sigma} + (1 - \langle \hat{\sigma} \rangle) \hat{\mathbb{1}}$ such that $\langle \hat{\sigma} \rangle = 1$ at all times. Then, the optimal readout is given by

$$r^* = \frac{1}{2} \left\langle \left[\hat{L}, \hat{\sigma} \right]_+ \right\rangle. \quad (\text{A11})$$

The equations for optimal paths take the form

$$\begin{aligned} \frac{\partial \hat{\rho}}{\partial t} &= -i[\hat{H}, \hat{\rho}] - \frac{1}{4\tau} [\Delta\hat{V}, \hat{\rho}]_+ + \frac{r^*}{2\tau} [\Delta\hat{L}, \hat{\rho}]_+, \\ \frac{\partial \hat{\sigma}}{\partial t} &= -i[\hat{H}, \hat{\sigma}] + \frac{1}{4\tau} [\Delta\hat{V}, \hat{\sigma}]_+ - \frac{r^*}{2\tau} [\Delta\hat{L}, \hat{\sigma}]_+. \end{aligned} \quad (\text{A12})$$

The optimal Hamiltonian is

$$\begin{aligned} \mathcal{H}^*(\hat{\sigma}, \hat{\rho}) &= \left\langle i[\hat{H}, \hat{\sigma}] \right\rangle + \frac{1}{8\tau} \left\langle \left[\Delta\hat{L}, \hat{\sigma} \right]_+ \right\rangle^2 \\ &\quad - \frac{1}{4\tau} \left\langle \left[(\Delta\hat{L})^2, \hat{\sigma} \right]_+ \right\rangle \\ &= \left\langle i[\hat{H}, \hat{\sigma}] \right\rangle + \frac{1}{8\tau} \left\langle \left[\hat{L}, \hat{\sigma} \right]_+ \right\rangle^2 \\ &\quad - \frac{1}{4\tau} \left\langle \left[\hat{V}, \hat{\sigma} \right]_+ \right\rangle. \end{aligned} \quad (\text{A13})$$

The optimal path equations in Eq. (A12) can be found from the optimal Hamiltonian and can be expressed as

$$\frac{\partial \hat{\rho}}{\partial t} = \frac{\delta \mathcal{H}^*}{\delta \hat{\sigma}}, \quad \frac{\partial \hat{\sigma}}{\partial t} = -\frac{\delta \mathcal{H}^*}{\delta \hat{\rho}}, \quad (\text{A14})$$

where the derivatives above denote functional derivatives.

Appendix B: Time evolution identities

This appendix provides formulae for the evolution of different expectation values along the optimal paths. Assume \hat{B}_χ is an explicitly time-dependent observable in general dependent on control χ as well. Similarly, we introduce the subscript χ to denote the control dependence of the observables and the optimal readouts in Eqs. (A11) and (A12). We also define the anti-commutator and the commutator of the state and costate as

$$\hat{\Omega} = \frac{1}{2} [\hat{\rho}, \hat{\sigma}]_+, \quad \hat{\Lambda} = [\hat{\rho}, \hat{\sigma}]. \quad (\text{B1})$$

Note that $\text{Tr } \hat{\Omega} = 1$ and $\text{Tr } \hat{\Lambda} = 0$. We can show the following identities

$$\begin{aligned} \frac{d\langle \hat{B}_\chi \rangle}{dt} &= \left\langle \frac{\partial \hat{B}_\chi}{\partial t} + \dot{\chi} \frac{\partial \hat{B}_\chi}{\partial \chi} \right\rangle + \\ &\left\langle i [\hat{H}_\chi, \hat{B}_\chi] - \frac{1}{4\tau} [\Delta \hat{V}_\chi, \hat{B}_\chi]_+ + \frac{r_\chi}{2\tau} [\Delta \hat{L}_\chi, \hat{B}_\chi]_+ \right\rangle \\ &= \left\langle \frac{\partial \hat{B}_\chi}{\partial t} + \dot{\chi} \frac{\partial \hat{B}_\chi}{\partial \chi} + i [\hat{H}_\chi, \hat{B}_\chi] + \frac{1}{2\tau} \langle \Delta \hat{L}_\chi^2 \rangle \hat{B}_\chi \right\rangle \\ &+ \left\langle -\frac{1}{4\tau} [\Delta \hat{L}_\chi^2, \hat{B}_\chi]_+ + \frac{r_\chi - \langle \hat{L}_\chi \rangle}{2\tau} [\Delta \hat{L}_\chi, \hat{B}_\chi]_+ \right\rangle \\ &= \left\langle \frac{\partial \hat{B}_\chi}{\partial t} + \dot{\chi} \frac{\partial \hat{B}_\chi}{\partial \chi} + i [\hat{H}_\chi, \hat{B}_\chi] \right\rangle + \\ &\left\langle -\frac{1}{4\tau} [\Delta \hat{L}_\chi^2, \Delta \hat{B}_\chi]_+ + \frac{r_\chi - \langle \hat{L}_\chi \rangle}{2\tau} [\Delta \hat{L}_\chi, \Delta \hat{B}_\chi]_+ \right\rangle, \end{aligned} \quad (\text{B2a})$$

$$\begin{aligned} \frac{d\text{Tr}(\hat{B}_\chi \hat{\Omega})}{dt} &= \text{Tr} \left(\left(\frac{\partial \hat{B}_\chi}{\partial t} + \dot{\chi} \frac{\partial \hat{B}_\chi}{\partial \chi} + i [\hat{H}_\chi, \hat{B}_\chi] \right) \hat{\Omega} \right) \\ &+ \frac{1}{8\tau} \text{Tr}([\hat{V}_\chi, \hat{B}_\chi] \hat{\Lambda}) - \frac{r_\chi}{4\tau} \text{Tr}([\hat{L}_\chi, \hat{B}_\chi] \hat{\Lambda}), \end{aligned} \quad (\text{B2b})$$

$$\begin{aligned} \frac{d\text{Tr}(\hat{B}_\chi \hat{\Lambda})}{dt} &= \text{Tr} \left(\left(\frac{\partial \hat{B}_\chi}{\partial t} + \dot{\chi} \frac{\partial \hat{B}_\chi}{\partial \chi} + i [\hat{H}_\chi, \hat{B}_\chi] \right) \hat{\Lambda} \right) \\ &+ \frac{1}{2\tau} \text{Tr}([\hat{V}_\chi, \hat{B}_\chi] \hat{\Omega}) - \frac{r_\chi}{\tau} \text{Tr}([\hat{L}_\chi, \hat{B}_\chi] \hat{\Omega}), \end{aligned} \quad (\text{B2c})$$

where $\Delta \hat{O} = \hat{O} - \langle \hat{O} \rangle$, for any observable \hat{O} . Note that $\text{Tr}(\hat{L}_\chi \hat{\Omega}) = r_\chi$. If $\hat{B}_\chi = \hat{L}_\chi$ with no explicit time dependence, Eq. (B2b) leads to

$$\frac{dr_\chi}{dt} = \text{Tr} \left(\left(\dot{\chi} \frac{\partial \hat{L}_\chi}{\partial \chi} + i [\hat{H}_\chi, \hat{L}_\chi] \right) \hat{\Omega} \right). \quad (\text{B3})$$

Note, under quantum nondemolition measurements, with no control, $\frac{dr_\chi}{dt} = 0$. Thus, the most likely readout is constant for quantum nondemolition measurements.

For arbitrary $\hat{A}_\chi, \hat{B}_\chi$ operators, we adopt the following notations

$$\hat{C}_\chi^{AB} = \frac{1}{2} [\Delta \hat{A}_\chi, \Delta \hat{B}_\chi]_+. \quad (\text{B4})$$

Therefore,

$$\text{Cov}(\hat{A}_\chi, \hat{B}_\chi) = \langle \hat{C}_\chi^{AB} \rangle. \quad (\text{B5})$$

We also denote

$$\frac{\partial}{\partial t} + \dot{\chi} \frac{\partial}{\partial \chi} = \partial_\eta, \quad \hat{N}_\chi = -\frac{1}{4\tau} \Delta \hat{L}_\chi^2 + \frac{r_\chi - \langle \hat{L}_\chi \rangle}{2\tau} \Delta \hat{L}_\chi. \quad (\text{B6})$$

We can show that

$$\begin{aligned} \frac{d\langle \hat{C}_\chi^{AB} \rangle}{dt} &= \left\langle \partial_\eta \hat{C}_\chi^{AB} + i [\hat{H}_\chi, \hat{C}_\chi^{AB}] + \frac{\langle \Delta \hat{L}_\chi^2 \rangle}{2\tau} \hat{C}_\chi^{AB} \right\rangle \\ &+ \left\langle [\hat{N}_\chi, \hat{C}_\chi^{AB}]_+ \right\rangle \\ &= \text{Cov}(\partial_\eta \hat{A}_\chi, \hat{B}_\chi) + \text{Cov}(\hat{A}_\chi, \partial_\eta \hat{B}_\chi) \\ &+ \left\langle i [\hat{H}_\chi, \hat{C}_\chi^{AB}] + \frac{\langle \Delta \hat{L}_\chi^2 \rangle}{2\tau} \hat{C}_\chi^{AB} + [\hat{N}_\chi, \hat{C}_\chi^{AB}]_+ \right\rangle. \end{aligned} \quad (\text{B7})$$

The above equation is consistent with $\langle \hat{B}_\chi \rangle$ evolution.

Appendix C: Optimal path for the quantum harmonic oscillator

For a simple harmonic oscillator with Hamiltonian given by Eq. (16), and quadratures Eqs. (17) and (18), we can write

$$\hat{H} = \frac{1}{2} (\hat{L}_\theta^2 + \hat{M}_\theta^2). \quad (\text{C1})$$

The following identities are true

$$\begin{aligned} [\hat{L}_\theta, \hat{M}_\theta] &= i, \quad [\hat{H}, \hat{L}_\theta] = -i\hat{M}_\theta, \quad [\hat{H}, \hat{M}_\theta] = i\hat{L}_\theta, \\ [\hat{L}_\theta^2, \hat{M}_\theta] &= 2i\hat{L}_\theta, \quad \frac{\partial \hat{L}_\theta}{\partial \theta} = \hat{M}_\theta, \quad \frac{\partial \hat{M}_\theta}{\partial \theta} = -\hat{L}_\theta. \end{aligned} \quad (\text{C2})$$

From Eq. (A11) and (B1), the optimal readout for adaptive quadrature measurement can be written as

$$r_\theta = \frac{1}{2} \left\langle [\hat{L}_\theta, \hat{\sigma}]_+ \right\rangle = \text{Tr}(\hat{L}_\theta \hat{\Omega}). \quad (\text{C3})$$

From Eq. (B3), we can derive

$$\frac{dr_\theta}{dt} = \dot{\phi} \text{Tr}(\hat{M}_\theta \hat{\Omega}), \quad (\text{C4})$$

where $\dot{\phi} = \dot{\theta} + 1$. Now we assume $v_\theta = \text{Tr}(\hat{M}_\theta \hat{\Omega})$. The evolution of v_θ can be derived from Eq. (B2b) to be

$$\frac{dv_\theta}{dt} = -\dot{\phi} r_\theta + \frac{i}{4\tau} \text{Tr}(\hat{L}_\theta \hat{\Lambda}). \quad (\text{C5})$$

We denote $w_\theta = i \langle [\hat{\sigma}, \hat{L}_\theta] \rangle = i \text{Tr}(\hat{L}_\theta \hat{\Lambda})$. From Eq. (B2c), we get

$$\frac{dw_\theta}{dt} = i \dot{\phi} \text{Tr}(\hat{M}_\theta \hat{\Lambda}). \quad (\text{C6})$$

Similarly, with the definition $z_\theta = i \langle [\hat{\sigma}, \hat{M}_\theta] \rangle = i \text{Tr}(\hat{M}_\theta \hat{\Lambda})$

$$\frac{dz_\theta}{dt} = -\dot{\phi} w_\theta. \quad (\text{C7})$$

Thus, the evolution of the optimal noise can be expressed in terms of the following coupled equations

$$\frac{dr_\theta}{dt} = \dot{\phi}v_\theta \quad (\text{C8a})$$

$$\frac{dv_\theta}{dt} = -\dot{\phi}r_\theta + \frac{w_\theta}{4\tau}, \quad (\text{C8b})$$

$$\frac{dw_\theta}{dt} = \dot{\phi}z_\theta, \quad \frac{dz_\theta}{dt} = -\dot{\phi}w_\theta, \quad (\text{C8c})$$

with $\dot{\phi} = \dot{\theta} + 1$.

Appendix D: Numerical Methods for monitored oscillator undergoing position measurements

We first consider the numerical methods for finding the optimal paths for oscillators undergoing position measurements (i.e. $\theta(t) = 0$, see Fig. 2). The most likely state evolution in Eq. (21a) can be expressed as

$$\frac{\partial \hat{\rho}}{\partial t} = \hat{F}\hat{\rho} + \hat{\rho}\hat{F}^\dagger, \quad (\text{D1})$$

with $\hat{F} = -i\hat{H} - \frac{1}{4\tau}\Delta\hat{V}_\theta + \frac{r_\theta}{2\tau}\Delta\hat{L}_\theta$. We take r_θ to be of the form given by Eq. (26), with the complex constant α and real constants A and B to be determined. To integrate Eq. (D1), $\hat{\rho}(t + dt)$ is expressed as

$$\hat{\rho}(t + dt) = \frac{\hat{\rho}'}{\text{Tr}\hat{\rho}'}, \quad (\text{D2})$$

with

$$\hat{\rho}' = \hat{U}_{dt}\hat{M}_{dt}\hat{\rho}\hat{M}_{dt}^\dagger\hat{U}_{dt}^\dagger, \quad (\text{D3})$$

where \hat{M}_{dt} is the Stratonovich form of the Kraus operator

$$\hat{M}_{dt} = \hat{1} + \frac{rdt}{2\tau}\hat{L} - \frac{dt}{4\tau}\hat{L}^2. \quad (\text{D4})$$

The above form ensures the positivity of the density matrix throughout the simulation [148]. We find α , A and B (see Eq. (26)) by maximizing the fidelity between the target final state $\hat{\rho}_f$ and the simulated final state $\hat{\rho}(t_f)$, defined as

$$\mathcal{F}(t_f, \hat{\rho}_f) = \text{Tr}(\hat{\rho}(t_f)\hat{\rho}_f). \quad (\text{D5})$$

We can adopt the above definition of fidelity since we restrict our analysis to pure states.

Appendix E: Relevant equations for a monitored parametric oscillator

We recall McCoy's formula for position and momentum commutation [149]

$$[\hat{X}^n, \hat{P}^m] = \sum_{k=1}^{\min(n,m)} C(n, m, k) \hat{X}^{n-k} \hat{P}^{m-k}, \quad (\text{E1})$$

where

$$C(n, m, k) = \begin{cases} \frac{-(-i)^k n! m!}{k!(n-k)!(m-k)!} & \text{for } k \leq n, m \\ 0 & \text{otherwise.} \end{cases} \quad (\text{E2})$$

From now on, we will assume the sum in Eq. (E1) starts from $k = 1$ without explicitly mentioning it. For a Hamiltonian

$$\hat{H} = \frac{1}{2}(\hat{X}^2 + \hat{P}^2) + \lambda_1(t)\hat{X}^2 + \lambda_2(t)\hat{X}^3, \quad (\text{E3})$$

and \hat{L}_θ defined in Eq. (17), the following identities are true.

$$\begin{aligned} [\hat{H}, \hat{X}^n \hat{P}^m] &= \sum_k \left(\frac{1}{2}(1 + 2\lambda_1)C(2, m, k) \hat{X}^{n+2-k} \hat{P}^{m-k} \right. \\ &\quad \left. + \lambda_2 C(3, m, k) \hat{X}^{n+3-k} \hat{P}^{m-k} \right. \\ &\quad \left. - \frac{1}{2}C(n, 2, k) \hat{X}^{n-k} \hat{P}^{m+2-k} \right), \end{aligned} \quad (\text{E4a})$$

$$\begin{aligned} [\hat{L}_\theta, \hat{X}^n \hat{P}^m] &= \sum_k \left(\cos\theta C(1, m, k) \hat{X}^{n+1-k} \hat{P}^{m-k} \right. \\ &\quad \left. - \sin\theta C(n, 1, k) \hat{X}^{n-k} \hat{P}^{m+1-k} \right), \end{aligned} \quad (\text{E4b})$$

$$\begin{aligned} [\hat{L}_\theta^2, \hat{X}^n \hat{P}^m] &= \sum_k \left(\cos^2\theta C(2, m, k) \hat{X}^{n+2-k} \hat{P}^{m-k} \right. \\ &\quad \left. + 2\sin\theta \cos\theta (C(1, m, k) - C(n, 1, k)) \right. \\ &\quad \left. \times \hat{X}^{n+1-k} \hat{P}^{m+1-k} \right. \\ &\quad \left. - \sin^2\theta C(n, 2, k) \hat{X}^{n-k} \hat{P}^{m+2-k} \right). \end{aligned} \quad (\text{E4c})$$

We define the following scalars

$$\begin{aligned} \Gamma(n, m) &= \text{Tr}(\hat{X}^n \hat{P}^m \hat{\Omega}), \\ \kappa(n, m) &= i \text{Tr}(\hat{X}^n \hat{P}^m \hat{\Lambda}). \end{aligned} \quad (\text{E5})$$

Using Eqs. (B2) and (E4), we can derive the following recurrence relations

$$\begin{aligned}
\frac{d\Gamma(n, m)}{dt} = i \sum_{k=1} \left[\left(\frac{1}{2}(1 + 2\lambda_1)C(2, m, k)\Gamma(n + 2 - k, m - k) + \lambda_2 C(3, m, k)\Gamma(n + 3 - k, m - k) \right. \right. \\
\left. \left. - \frac{1}{2}C(n, 2, k)\Gamma(n - k, m + 2 - k), \right) - \frac{1}{8\tau} \left(\cos^2 \theta C(2, m, k)\kappa(n + 2 - k, m - k) \right. \right. \\
\left. \left. + 2 \sin \theta \cos \theta (C(1, m, k) - C(n, 1, k))\kappa(n + 1 - k, m + 1 - k) \right. \right. \\
\left. \left. - \sin^2 \theta C(n, 2, k)\kappa(n - k, m + 2 - k), \right) + \frac{r\theta}{4\tau} \left(\cos \theta C(1, m, k)\kappa(n + 1 - k, m - k) \right. \right. \\
\left. \left. - \sin \theta C(n, 1, k)\kappa(n - k, m + 1 - k) \right) \right], \tag{E6a}
\end{aligned}$$

$$\begin{aligned}
\frac{d\kappa(n, m)}{dt} = i \sum_{k=1} \left[\left(\frac{1}{2}(1 + 2\lambda_1)C(2, m, k)\kappa(n + 2 - k, m - k) + \lambda_2 C(3, m, k)\kappa(n + 3 - k, m - k) \right. \right. \\
\left. \left. - \frac{1}{2}C(n, 2, k)\kappa(n - k, m + 2 - k), \right) + \frac{1}{2\tau} \left(\cos^2 \theta C(2, m, k)\Gamma(n + 2 - k, m - k) \right. \right. \\
\left. \left. + 2 \sin \theta \cos \theta (C(1, m, k) - C(n, 1, k))\Gamma(n + 1 - k, m + 1 - k) \right. \right. \\
\left. \left. - \sin^2 \theta C(n, 2, k)\Gamma(n - k, m + 2 - k), \right) - \frac{r\theta}{\tau} \left(\cos \theta C(1, m, k)\Gamma(n + 1 - k, m - k) \right. \right. \\
\left. \left. - \sin \theta C(n, 1, k)\Gamma(n - k, m + 1 - k) \right) \right], \tag{E6b}
\end{aligned}$$

with $\Gamma(0, 0) = 1$ and $\kappa(0, 0) = 0$. Also, the optimal readout r_θ can be written as

$$r_\theta = \cos \theta \Gamma(1, 0) + \sin \theta \Gamma(0, 1). \tag{E7}$$

We define the order of $\Gamma(n, m)$ or $\kappa(n, m)$ to be $n + m$. Note that in Eqs. (E6), only the terms multiplied by λ_2 lead to an increase in the order (since $k \geq 1$). Therefore, the model reduction strategy presented in secs. II C and III B only works when the oscillator does not have any anharmonic potential. We can write the optimal Hamiltonian from Eq. (15) as

$$\begin{aligned}
\mathcal{H}^*(\hat{\sigma}, \hat{\rho}, \theta, \lambda_1, \lambda_2) = -i \text{Tr} \left(\hat{H} \hat{\Lambda} \right) + \frac{1}{2\tau} \left(\text{Tr} \left(\hat{L}_\theta \hat{\Omega} \right) \right)^2 \\
- \frac{1}{2\tau} \text{Tr} \left(\hat{L}_\theta^2 \hat{\Omega} \right), \tag{E8}
\end{aligned}$$

which can be expanded as

$$\begin{aligned}
\mathcal{H}^* = - \left(\frac{1}{2}(1 + 2\lambda_1)\kappa(2, 0) + \frac{1}{2}\kappa(0, 2) + \lambda_2 \kappa(3, 0) \right) \\
+ \frac{1}{2\tau} \left(\cos \theta \Gamma(1, 0) + \sin \theta \Gamma(0, 1) \right)^2 \\
- \frac{1}{2\tau} \left(\cos^2 \theta \Gamma(2, 0) + \cos \theta \sin \theta (2\Gamma(1, 1) - i) \right. \\
\left. + \sin^2 \theta \Gamma(0, 2) \right). \tag{E9}
\end{aligned}$$

Assuming $\lambda_1 \in [-\lambda_1^{\max}, \lambda_1^{\max}]$ and $\lambda_2 \in [-\lambda_2^{\max}, \lambda_2^{\max}]$, according to Eq. (37), the optimal values of these parameters are

$$\lambda_1 = -\lambda_1^{\max} \text{sign}(\kappa(2, 0)), \quad \lambda_2 = -\lambda_2^{\max} \text{sign}(\kappa(3, 0)). \tag{E10}$$

Thus, we get a bang-bang form of optimal control. Eq. (E9) then becomes

$$\begin{aligned}
\mathcal{H}^* = \lambda_1^{\max} |\kappa(2, 0)| + \lambda_2^{\max} |\kappa(3, 0)| - \frac{1}{2} \left(\kappa(2, 0) + \kappa(0, 2) \right) \\
+ \frac{1}{4\tau} \left(\Gamma(1, 0)^2 + \Gamma(0, 1)^2 - \Gamma(2, 0) - \Gamma(0, 2) \right) \\
+ \frac{1}{2\tau} \left(A_\Gamma \cos 2\theta + B_\Gamma \sin 2\theta \right), \tag{E11}
\end{aligned}$$

where

$$\begin{aligned} A_\Gamma &= \frac{1}{2} \left(\Gamma(1,0)^2 - \Gamma(0,1)^2 - \Gamma(2,0) + \Gamma(0,2) \right) \\ B_\Gamma &= \Gamma(1,0)\Gamma(0,1) - \Gamma(1,1) + \frac{i}{2}. \end{aligned} \quad (\text{E12})$$

Note that both A_Γ and B_Γ are real. We define $A_\Gamma = R_\Gamma \cos \phi_\Gamma$ and $B_\Gamma = R_\Gamma \sin \phi_\Gamma$ such that $R_\Gamma = \sqrt{A_\Gamma^2 + B_\Gamma^2} \geq 0$. Then Eq. (E11) can be written as

$$\begin{aligned} \mathcal{H}^* &= \lambda_1^{\max} |\kappa(2,0)| + \lambda_2^{\max} |\kappa(3,0)| - \frac{1}{2} \left(\kappa(2,0) + \kappa(0,2) \right) \\ &+ \frac{1}{2\tau} \left(\Gamma(1,0)^2 + \Gamma(0,1)^2 - \Gamma(2,0) - \Gamma(0,2) \right) \\ &+ \frac{1}{2\tau} R_\Gamma \cos(2\theta - \phi_\Gamma). \end{aligned} \quad (\text{E13})$$

Assuming $\phi_\Gamma \in [-\pi, \pi]$ and $\theta \in [-\frac{\pi}{2}, \frac{\pi}{2}]$, supremum is achieved for

$$\theta = \frac{1}{2} \phi_\Gamma, \quad (\text{E14})$$

where the value of ϕ_Γ is determined by A_Γ , B_Γ and their signs. The supremum value of the Pontryagin Hamiltonian is

$$\begin{aligned} \mathcal{K}(\hat{\sigma}, \hat{\rho}) &= \lambda_1^{\max} |\kappa(2,0)| + \lambda_2^{\max} |\kappa(3,0)| + \frac{1}{2\tau} R_\Gamma \\ &- \frac{1}{2} \left(\kappa(2,0) + \kappa(0,2) \right) \\ &+ \frac{1}{2\tau} \left(\Gamma(1,0)^2 + \Gamma(0,1)^2 - \Gamma(2,0) - \Gamma(0,2) \right). \end{aligned} \quad (\text{E15})$$

From Eqs. (E6) we can calculate the evolution of the coefficients appearing above. Then,

$$\frac{d\Gamma(1,0)}{dt} = \Gamma(0,1) - \frac{\sin \theta}{4\tau} (\cos \theta \kappa(1,0) + \sin \theta \kappa(0,1)), \quad (\text{E16a})$$

$$\begin{aligned} \frac{d\Gamma(0,1)}{dt} &= - (1 + 2\lambda_1)\Gamma(1,0) - 3\lambda_2\Gamma(2,0) \\ &+ \frac{\cos \theta}{4\tau} (\cos \theta \kappa(1,0) + \sin \theta \kappa(0,1)), \end{aligned} \quad (\text{E16b})$$

$$\frac{d\kappa(1,0)}{dt} = \kappa(0,1), \quad (\text{E16c})$$

$$\frac{d\kappa(0,1)}{dt} = - (1 + 2\lambda_1)\kappa(1,0) - 3\lambda_2\kappa(2,0). \quad (\text{E16d})$$

We denote $\tilde{\Gamma}(1,1) = \Gamma(1,1) - \frac{i}{2}$, $\tilde{\Gamma}(2,1) = \Gamma(2,1) - i\Gamma(1,0)$, $\tilde{\kappa}(2,1) = \kappa(2,1) - i\kappa(1,0)$ to ensure the scalar variables are all real. The second order Γ terms evolve

as

$$\begin{aligned} \frac{d\Gamma(2,0)}{dt} &= 2\tilde{\Gamma}(1,1) + \\ &\frac{\sin \theta}{2\tau} \left(\cos \theta \left(\Gamma(1,0)\kappa(1,0) - \kappa(2,0) \right) \right. \\ &\left. + \sin \theta \left(\Gamma(0,1)\kappa(1,0) - \kappa(1,1) \right) \right), \end{aligned} \quad (\text{E17a})$$

$$\begin{aligned} \frac{d\tilde{\Gamma}(1,1)}{dt} &= - (1 + 2\lambda_1)\Gamma(2,0) + \Gamma(0,2) - 3\lambda_2\Gamma(3,0) + \\ &\frac{1}{4\tau} \left(r_\theta \times \left(\sin \theta \kappa(0,1) - \cos \theta \kappa(1,0) \right) \right. \\ &\left. + \left(\cos^2 \theta \kappa(2,0) - \sin^2 \theta \kappa(0,2) \right) \right), \end{aligned} \quad (\text{E17b})$$

$$\begin{aligned} \frac{d\Gamma(0,2)}{dt} &= - 2(1 + 2\lambda_1)\tilde{\Gamma}(1,1) - 6\lambda_2\tilde{\Gamma}(2,1) \\ &+ \frac{\cos \theta}{2\tau} \left(\left(\sin \theta \kappa(0,2) + \cos \theta \kappa(1,1) \right) \right. \\ &\left. - \left(\cos \theta \Gamma(1,0) + \sin \theta \Gamma(0,1) \right) \kappa(0,1) \right), \end{aligned} \quad (\text{E17c})$$

The second order κ terms evolve according to the following equations.

$$\begin{aligned} \frac{d\kappa(2,0)}{dt} &= 2\kappa(1,1) + \\ &\frac{2 \sin \theta}{\tau} \left(\cos \theta \Gamma(2,0) + \sin \theta \tilde{\Gamma}(1,1) - r_\theta \Gamma(1,0) \right), \end{aligned} \quad (\text{E18a})$$

$$\begin{aligned} \frac{d\kappa(1,1)}{dt} &= - (1 + 2\lambda_1)\kappa(2,0) + \kappa(0,2) - 3\lambda_2\kappa(3,0) + \\ &\frac{1}{\tau} \left(r_\theta \left(\cos \theta \Gamma(1,0) - \sin \theta \Gamma(0,1) \right) \right. \\ &\left. + \left(-\cos^2 \theta \Gamma(2,0) + \sin^2 \theta \Gamma(0,2) \right) \right), \end{aligned} \quad (\text{E18b})$$

$$\begin{aligned} \frac{d\kappa(0,2)}{dt} &= - 2(1 + 2\lambda_1)\kappa(1,1) - 6\lambda_2\tilde{\kappa}(2,1) \\ &+ \frac{2 \cos \theta}{\tau} \left(- \left(\sin \theta \Gamma(0,2) + \cos \theta \tilde{\Gamma}(1,1) \right) \right. \\ &\left. + \left(\cos \theta \Gamma(1,0) + \sin \theta \Gamma(0,1) \right) \Gamma(0,1) \right). \end{aligned} \quad (\text{E18c})$$

Appendix F: Numerical Methods for finding optimal control

We present the numerical methods adopted for finding the optimal $\theta(t)$ and $\lambda_1(t)$ (e.g. Fig. 3). We assume initial values of the 10 scalars $\Gamma(1,0)$, $\Gamma(0,1)$, $\kappa(1,0)$, $\kappa(0,1)$, $\Gamma(2,0)$, $\tilde{\Gamma}(1,1)$, $\Gamma(0,2)$, $\kappa(2,0)$, $\kappa(1,1)$ and $\kappa(0,2)$. At each step, the optimal controls are given by Eqs. (63) and (64). The step update is calculated according to the steps presented in appendix D with a fourth-order Runge-Kutta method [150]. The initial values of the scalars Γ and κ are solved so that the final state is the target state ρ_f . We express the density matrix in the fock state basis up to level $n = 35$. To that end, we maximize the fidelity in Eq. (D5). For maximization, we adopted simulated annealing [151] using JAX [152]. To ensure the solution is optimal (or near optimal), after a certain fidelity is reached (90-95%), we only accept solutions if the cost function in Eq. (45) is further reduced. Therefore, the problem becomes a Pareto front optimization between the fidelity with respect to the target state and readout probabilities. Robust numerical methods to find optimal solutions should be investigated in the future. The codes for finding optimal control are available at [153].

Appendix G: Numerical method for generating stochastic trajectories

We present the numerical methods adopted for generating stochastic trajectories with given initial state $\hat{\rho}_i$ and control. We use the Itô form of the stochastic master Eq. (19), given by

$$\frac{\partial \hat{\rho}}{\partial t} = -i[\hat{H}, \hat{\rho}] + \frac{1}{4\tau} \mathcal{D}_{\hat{L}_\theta}[\hat{\rho}] + \frac{1}{2\tau} [\Delta \hat{L}_\theta, \hat{\rho}]_+, \quad (\text{G1})$$

with

$$\mathcal{D}_{\hat{L}_\theta}[\hat{\rho}] = \hat{L}_\theta \hat{\rho} \hat{L}_\theta - \frac{1}{2} \hat{L}_\theta^2 \hat{\rho} - \frac{1}{2} \hat{\rho} \hat{L}_\theta^2. \quad (\text{G2})$$

To preserve the positivity, we approximate the stochastic master equation as

$$\hat{\rho}(t+dt) \approx \frac{\hat{\rho}'}{\text{Tr} \hat{\rho}'}, \quad (\text{G3})$$

with

$$\hat{\rho}' = \hat{M}_{\text{It}\hat{\rho}} \hat{\rho} \hat{M}_{\text{It}\hat{\rho}}^\dagger, \quad (\text{G4})$$

and

$$\hat{M}_{\text{It}\hat{\rho}} \approx \hat{1} - i\hat{H}dt + \frac{rdt}{2\tau} \hat{L}_\theta - \frac{dt}{8\tau} \hat{L}_\theta^2, \quad (\text{G5})$$

is the measurement Kraus operator in Itô form. Eq. (G3) is the same as (G1) as the latter can be derived using the Kraus operator in Eq. (G5) and expanding up to $\mathcal{O}(dt)$ with the Itô rule $dW^2 = dt$ in mind. At each time step, we generate a Gaussian random number with mean 0 and variance dt as the Wiener noise dW and integrate Eq. (G3).

Appendix H: Numerical method for generating a sample control

In this section, we discuss the method of generating a sample control between $\hat{\rho}_i$ and $\hat{\rho}_f$ for a monitored harmonic oscillator. We first express the sample parameters as follows

$$\theta(t) = \frac{\pi}{2} \tanh \frac{2f_1(t)}{\pi}, \quad \lambda_1(t) = \lambda_1^{\max} \tanh \frac{f_2(t)}{\lambda_1^{\max}}, \quad (\text{H1})$$

where $f_1(t)$ and $f_2(t)$ are expressed in terms of Fourier series as below

$$f_1(t) = \sum_{n=0}^{N_c} \left(c_n \cos \frac{2\pi n(t-t_i)}{t_f-t_i} + d_n \sin \frac{2\pi n(t-t_i)}{t_f-t_i} \right), \quad (\text{H2a})$$

$$f_2(t) = \sum_{n=0}^{N_c} \left(c'_n \cos \frac{2\pi n(t-t_i)}{t_f-t_i} + d'_n \sin \frac{2\pi n(t-t_i)}{t_f-t_i} \right). \quad (\text{H2b})$$

The hyperbolic tangents in Eq. (H1) make sure the controls $\theta(t)$ and $\lambda_1(t)$ are bounded by $\frac{\pi}{2}$ and λ_1^{\max} . For $|\frac{2f_1(t)}{\pi}| \ll 1$, $\theta_1(t) \simeq f_1(t)$. Similarly, for $|\frac{f_2(t)}{\lambda_1^{\max}}| \ll 1$, $\lambda_1(t) \simeq f_2(t)$. For our simulations, $N_c = 5$ is sufficient. We integrate Eq. (21a) (with the Hamiltonian given by Eq. (56)) and Eqs. (59) for the controls in Eq. (H1). We maximize the fidelity defined in Eq. (D5) with respect to coefficients $\{c_n, d_n, c'_n, d'_n\}$ using simulated annealing. Assuming we can reach fidelity close to 100%, the solution obtained this way is the most likely path between $\hat{\rho}_i$ and $\hat{\rho}_f$ under the controls defined in Eqs. (H1). The controls obtained this way are usually not optimal, as shown in the text.

Appendix I: Position Measurement

For only position measurement, $\theta(t) = 0$ in Eq. (17). As $t \rightarrow \infty$, the covariance matrix elements of a Gaussian state harmonic oscillator reach steady state values. Adopting the notation from Ref. [54], we denote $q_1 = \langle \hat{X} \rangle$, $q_2 = \langle \hat{P} \rangle$, $q_3 = 2\text{Var} \hat{X}$, $q_4 = 2\text{Cov}(\hat{X}, \hat{P})$, and $q_5 = 2\text{Var} \hat{P}$. The steady state values of q_3 , q_4 and q_5 are given by

$$\begin{aligned} \tilde{q}_3 &= \sqrt{4\tau(\sqrt{1+4\tau^2}-2\tau)}, \\ \tilde{q}_4 &= \sqrt{1+4\tau^2}-2\tau, \\ \tilde{q}_5 &= \sqrt{\frac{1}{\tau}(\sqrt{1+4\tau^2}-2\tau)(1+4\tau^2)}. \end{aligned} \quad (\text{I1})$$

The final state is a squeezed state with squeezing parameter $\xi = Re^{i\Theta}$ such that

$$\begin{aligned} \sinh 2R &= \pm \sqrt{\left(\frac{\tilde{q}_5 - \tilde{q}_3}{2}\right)^2 + \tilde{q}_4^2}, \\ \cosh 2R &= \frac{\tilde{q}_5 + \tilde{q}_3}{2}, \quad R = \frac{1}{2} \log(\sinh 2R + \cosh 2R). \end{aligned} \quad (12)$$

Then,

$$\xi = R(\cos \Theta + i \sin \Theta) = \frac{R}{\sinh 2R} \left(\frac{\tilde{q}_5 - \tilde{q}_3}{2} - i\tilde{q}_4 \right). \quad (13)$$

Note that either choice of sign in Eq. (12) leads to the same ξ .

Now consider an optimal path starting from (q_{1i}, q_{2i}) and ending at (q_{1f}, q_{2f}) at $t = t_f$. The solution for the unique optimal path is given by [54]

$$\begin{aligned} q_1(t) &= \left(\frac{\alpha_1(\tilde{q}_3^2 + \tilde{q}_4^2)}{8\tau} t + q_{1i} \right) \cos t + \left(\frac{\alpha_2(\tilde{q}_3^2 + \tilde{q}_4^2)}{8\tau} t + q_{2i} + \frac{\alpha_1(\tilde{q}_3^2 - \tilde{q}_4^2)}{8\tau} + \frac{\tilde{q}_3\tilde{q}_4\alpha_2}{4\tau} \right) \sin t, \\ q_2(t) &= \left(\frac{\alpha_2(\tilde{q}_3^2 + \tilde{q}_4^2)}{8\tau} t + q_{2i} \right) \cos t - \left(\frac{\alpha_1(\tilde{q}_3^2 + \tilde{q}_4^2)}{8\tau} t + q_{1i} + \frac{\alpha_2(\tilde{q}_3^2 - \tilde{q}_4^2)}{8\tau} - \frac{\tilde{q}_3\tilde{q}_4\alpha_1}{4\tau} \right) \sin t, \end{aligned} \quad (14)$$

where, α_1 and α_2 are integration constants. Values of α 's can be determined from the final conditions through the matrix equation

$$\mathcal{A}(t_f) \begin{pmatrix} \alpha_1 \\ \alpha_2 \end{pmatrix} = \begin{pmatrix} q_{1f} - q_{1i} \cos t_f - q_{2i} \sin t_f \\ q_{2f} + q_{1i} \sin t_f - q_{2i} \cos t_f \end{pmatrix}. \quad (15)$$

The matrix $\mathcal{A}(\tau_f)$ is given by

$$\mathcal{A}(t_f) = \frac{1}{8\tau} \begin{pmatrix} (\tilde{q}_3^2 + \tilde{q}_4^2)t_f \cos t_f + (\tilde{q}_3^2 - \tilde{q}_4^2) \sin t_f & ((\tilde{q}_3^2 + \tilde{q}_4^2)t_f + 2\tilde{q}_3\tilde{q}_4) \sin t_f \\ -(\tilde{q}_3^2 + \tilde{q}_4^2)t_f + 2\tilde{q}_3\tilde{q}_4 \sin t_f & (\tilde{q}_3^2 + \tilde{q}_4^2)t_f \cos t_f - (\tilde{q}_3^2 - \tilde{q}_4^2) \sin t_f \end{pmatrix}, \quad (16)$$

and is always invertible.

-
- [1] John Preskill, “Quantum Computing in the NISQ era and beyond,” *Quantum* **2**, 79 (2018).
- [2] Steven M. Girvin, “Introduction to quantum error correction and fault tolerance,” *SciPost Phys. Lect. Notes*, 70 (2023).
- [3] Tameem Albash and Daniel A. Lidar, “Adiabatic quantum computation,” *Rev. Mod. Phys.* **90**, 015002 (2018).
- [4] Kishor Bharti, Alba Cervera-Lierta, Thi Ha Kyaw, Tobias Haug, Sumner Alperin-Lea, Abhinav Anand, Matthias Degroote, Hermanni Heimonen, Jakob S. Kottmann, Tim Menke, Wai-Keong Mok, Sukin Sim, Leong-Chuan Kwek, and Alán Aspuru-Guzik, “Noisy intermediate-scale quantum algorithms,” *Rev. Mod. Phys.* **94**, 015004 (2022).
- [5] Frank Verstraete, Michael M. Wolf, and J. Ignacio Cirac, “Quantum computation and quantum-state engineering driven by dissipation,” *Nature Physics* **5**, 633–636 (2009).
- [6] Patrick M. Harrington, Erich J. Mueller, and Kater W. Murch, “Engineered dissipation for quantum information science,” *Nature Reviews Physics* **4**, 660–671 (2022).
- [7] P. Magnard, P. Kurpiers, B. Royer, T. Walter, J.-C. Besse, S. Gasparinetti, M. Pechal, J. Heinsoo, S. Storz, A. Blais, and A. Wallraff, “Fast and unconditional all-microwave reset of a superconducting qubit,” *Phys. Rev. Lett.* **121**, 060502 (2018).
- [8] Vivek Maurya, Haimeng Zhang, Daria Kowsari, Andre Kuo, Darian M. Hartsell, Clark Miyamoto, Jocelyn Liu, Sadman Shanto, Evangelos Vlachos, Azarin Zarassi, Kater W. Murch, and Eli M. Levenson-Falk, “On-demand driven dissipation for cavity reset and cooling,” *PRX Quantum* **5**, 020321 (2024).
- [9] Z. Leghtas, S. Touzard, I. M. Pop, A. Kou, B. Vlastakis, A. Petrenko, K. M. Sliwa, A. Narla, S. Shankar, M. J. Hatridge, M. Reagor, L. Frunzio, R. J. Schoelkopf, M. Mirrahimi, and M. H. Devoret, “Confining the state of light to a quantum manifold by engineered two-photon loss,” *Science* **347**, 853–857 (2015).
- [10] Ziqian Li, Tanay Roy, Yao Lu, Eliot Kapit, and David I. Schuster, “Autonomous stabilization with programmable stabilized state,” *Nature Communications*

- 15, 6978 (2024).
- [11] Y. Lin, J. P. Gaebler, F. Reiter, T. R. Tan, R. Bowler, A. S. Sørensen, D. Leibfried, and D. J. Wineland, “Dissipative production of a maximally entangled steady state of two quantum bits,” *Nature* **504**, 415–418 (2013), publisher: Nature Publishing Group.
- [12] Daniel C. Cole, Stephen D. Erickson, Giorgio Zanonello, Karl P. Horn, Pan-Yu Hou, Jenny J. Wu, Daniel H. Slichter, Florentin Reiter, Christiane P. Koch, and Dietrich Leibfried, “Resource-efficient dissipative entanglement of two trapped-ion qubits,” *Phys. Rev. Lett.* **128**, 080502 (2022).
- [13] Jeffrey M. Gertler, Brian Baker, Juliang Li, Shruti Shiro, Jens Koch, and Chen Wang, “Protecting a bosonic qubit with autonomous quantum error correction,” *Nature* **590**, 243–248 (2021).
- [14] Ziqian Li, Tanay Roy, David Rodríguez Pérez, Kan-Heng Lee, Eliot Kapit, and David I. Schuster, “Autonomous error correction of a single logical qubit using two transmons,” *Nature Communications* **15**, 1681 (2024).
- [15] Daniel Malz, Georgios Styliaris, Zhi-Yuan Wei, and J. Ignacio Cirac, “Preparation of matrix product states with log-depth quantum circuits,” *Phys. Rev. Lett.* **132**, 040404 (2024).
- [16] Howard M. Wiseman and Gerard J. Milburn, *Quantum Measurement and Control* (Cambridge University Press, 2009).
- [17] Andrew N. Jordan and Irfan A. Siddiqi, *Quantum Measurement: Theory and Practice* (Cambridge University Press, 2024).
- [18] Todd A. Brun, “A simple model of quantum trajectories,” *American Journal of Physics* **70**, 719–737 (2002).
- [19] Kurt Jacobs and Daniel A. Steck, “A Straightforward Introduction to Continuous Quantum Measurement,” *Contemporary Physics* **47**, 279–303 (2006).
- [20] K. W. Murch, S. J. Weber, C. Macklin, and I. Siddiqi, “Observing single quantum trajectories of a superconducting quantum bit,” *Nature* **502**, 211–214 (2013).
- [21] D. Tan, S. J. Weber, I. Siddiqi, K. Mølmer, and K. W. Murch, “Prediction and retrodiction for a continuously monitored superconducting qubit,” *Phys. Rev. Lett.* **114**, 090403 (2015).
- [22] Ananda Roy, Liang Jiang, A. Douglas Stone, and Michel Devoret, “Remote entanglement by coherent multiplication of concurrent quantum signals,” *Phys. Rev. Lett.* **115**, 150503 (2015).
- [23] N. Roch, M. E. Schwartz, F. Motzoi, C. Macklin, R. Vijay, A. W. Eddins, A. N. Korotkov, K. B. Whaley, M. Sarovar, and I. Siddiqi, “Observation of measurement-induced entanglement and quantum trajectories of remote superconducting qubits,” *Phys. Rev. Lett.* **112**, 170501 (2014).
- [24] S. Hacoen-Gourgy, L. P. García-Pintos, L. S. Martin, J. Dressel, and I. Siddiqi, “Incoherent qubit control using the quantum zeno effect,” *Phys. Rev. Lett.* **120**, 020505 (2018).
- [25] Giorgio Colangelo, Ferran Martin Ciurana, Lorena C. Bianchet, Robert J. Sewell, and Morgan W. Mitchell, “Simultaneous tracking of spin angle and amplitude beyond classical limits,” *Nature* **543**, 525–528 (2017).
- [26] J. M. Boss, K. S. Cujia, J. Zopes, and C. L. Degen, “Quantum sensing with arbitrary frequency resolution,” *Science* **356**, 837–840 (2017).
- [27] Yijin Xie, Jianpei Geng, Huiyao Yu, Xing Rong, Ya Wang, and Jiangfeng Du, “Dissipative quantum sensing with a magnetometer based on nitrogen-vacancy centers in diamond,” *Phys. Rev. Appl.* **14**, 014013 (2020).
- [28] Nathan S. Williams and Andrew N. Jordan, “Entanglement genesis under continuous parity measurement,” *Phys. Rev. A* **78**, 062322 (2008).
- [29] Song Zhang, Leigh S. Martin, and K. Birgitta Whaley, “Locally optimal measurement-based quantum feedback with application to multiqubit entanglement generation,” *Phys. Rev. A* **102**, 062418 (2020).
- [30] Philippe Lewalle, Cyril Elouard, and Andrew N. Jordan, “Entanglement-preserving limit cycles from sequential quantum measurements and feedback,” *Phys. Rev. A* **102**, 062219 (2020).
- [31] Areeya Chantasri, Ivonne Guevara, Kiarn T. Laverick, and Howard M. Wiseman, “Unifying theory of quantum state estimation using past and future information,” *Physics Reports* **930**, 1–40 (2021).
- [32] Ivonne Guevara and Howard Wiseman, “Quantum state smoothing,” *Phys. Rev. Lett.* **115**, 180407 (2015).
- [33] Ivonne Guevara and Howard M. Wiseman, “Completely positive quantum trajectories with applications to quantum state smoothing,” *Phys. Rev. A* **102**, 052217 (2020).
- [34] Luis Cortez, Areeya Chantasri, Luis Pedro García-Pintos, Justin Dressel, and Andrew N. Jordan, “Rapid estimation of drifting parameters in continuously measured quantum systems,” *Phys. Rev. A* **95**, 012314 (2017).
- [35] Jason F. Ralph, Simon Maskell, and Kurt Jacobs, “Multiparameter estimation along quantum trajectories with sequential monte carlo methods,” *Phys. Rev. A* **96**, 052306 (2017).
- [36] Areeya Chantasri, Shengshi Pang, Teerawat Chalerm-pusitarak, and Andrew N. Jordan, “Quantum state tomography with time-continuous measurements: reconstruction with resource limitations,” *Quantum Studies: Mathematics and Foundations* **7**, 23–47 (2020).
- [37] H. M. Wiseman, “Quantum theory of continuous feedback,” *Phys. Rev. A* **49**, 2133–2150 (1994).
- [38] A. C. Doherty and K. Jacobs, “Feedback Control of Quantum Systems Using Continuous State Estimation,” *Phys. Rev. A* **60**, 2700–2711 (1999).
- [39] C. Sames, C. Hamsen, H. Chibani, P. A. Altin, T. Wilk, and G. Rempe, “Continuous parametric feedback cooling of a single atom in an optical cavity,” *Phys. Rev. A* **97**, 053404 (2018).
- [40] Z. K. Mineev, S. O. Mundhada, S. Shankar, P. Reinhold, R. Gutiérrez-Jáuregui, R. J. Schoelkopf, M. Mirrahimi, H. J. Carmichael, and M. H. Devoret, “To catch and reverse a quantum jump mid-flight,” *Nature* **570**, 200–204 (2019).
- [41] William P. Livingston, Machiel S. Blok, Emmanuel Flurin, Justin Dressel, Andrew N. Jordan, and Irfan Siddiqi, “Experimental demonstration of continuous quantum error correction,” *Nature Communications* **13**, 2307 (2022).
- [42] A. Chantasri, J. Dressel, and A. N. Jordan, “Action principle for continuous quantum measurement,” *Phys. Rev. A* **88**, 042110 (2013).
- [43] Areeya Chantasri and Andrew N. Jordan, “Stochastic Path-Integral Formalism for Continuous Quantum Measurement,” *Phys. Rev. A* **92**, 032125 (2015).

- [44] Areeya Chantasri, “Stochastic Path Integral Formalism for Continuous Quantum Measurement,” PhD Dissertation, University of Rochester (2016).
- [45] Andrew N. Jordan, Areeya Chantasri, Pierre Rouchon, and Benjamin Huard, “Anatomy of Fluorescence: Quantum Trajectory Statistics From Continuously Measuring Spontaneous Emission,” *Quantum Studies: Mathematics and Foundations* **3**, 237–263 (2016).
- [46] Philippe Lewalle, Sreenath K. Manikandan, Cyril Elouard, and Andrew N. Jordan, “Measuring fluorescence to track a quantum emitter’s state: a theory review,” *Contemporary Physics* **61**, 26–50 (2020).
- [47] Philippe Lewalle, Areeya Chantasri, and Andrew N. Jordan, “Prediction and Characterization of Multiple Extremal Paths in Continuously Monitored Qubits,” *Phys. Rev. A* **95**, 042126 (2017).
- [48] Philippe Lewalle, John Steinmetz, and Andrew N. Jordan, “Chaos in Continuously Monitored Quantum Systems: An Optimal-Path Approach,” *Phys. Rev. A* **98**, 012141 (2018).
- [49] Dominic Shea and Alessandro Romito, “Action formalism for geometric phases from self-closing quantum trajectories,” (2023), arXiv:2312.14760 [quant-ph].
- [50] Dominic Shea and Alessandro Romito, “Stochastic action for the entanglement of a noisy monitored two-qubit system,” (2024), arXiv:2403.08422 [quant-ph].
- [51] S. J. Weber, A. Chantasri, J. Dressel, A. N. Jordan, K. W. Murch, and I. Siddiqi, “Mapping the Optimal Route between Two Quantum States,” *Nature* **511**, 570–573 (2014).
- [52] M. Naghiloo, D. Tan, P. M. Harrington, P. Lewalle, A. N. Jordan, and K. W. Murch, “Quantum Caustics in Resonance-Fluorescence Trajectories,” *Phys. Rev. A* **96**, 053807 (2017).
- [53] Areeya Chantasri, Mollie E. Kimchi-Schwartz, Nicolas Roch, Irfan Siddiqi, and Andrew N. Jordan, “Quantum trajectories and their statistics for remotely entangled quantum bits,” *Phys. Rev. X* **6**, 041052 (2016).
- [54] Tathagata Karmakar, Philippe Lewalle, and Andrew N. Jordan, “Stochastic path-integral analysis of the continuously monitored quantum harmonic oscillator,” *PRX Quantum* **3**, 010327 (2022).
- [55] Wirawat Kokaew, Thiparat Chotibut, and Areeya Chantasri, “Quantum state-preparation control in noisy environment via most-likely paths,” (2022), arXiv:2209.13164 [quant-ph].
- [56] Philippe Lewalle and K. Birgitta Whaley, “Pontryagin-optimal control of a non-hermitian qubit,” *Phys. Rev. A* **107**, 022216 (2023).
- [57] U. Boscain, M. Sigalotti, and D. Sugny, “Introduction to the pontryagin maximum principle for quantum optimal control,” *PRX Quantum* **2**, 030203 (2021).
- [58] Philippe Lewalle, Yipei Zhang, and K. Birgitta Whaley, “Optimal zeno dragging for quantum control: A shortcut to zero with action-based scheduling optimization,” *PRX Quantum* **5**, 020366 (2024).
- [59] Marios H. Michael, Matti Silveri, R. T. Brierley, Victor V. Albert, Juha Salmilehto, Liang Jiang, and S. M. Girvin, “New class of quantum error-correcting codes for a bosonic mode,” *Phys. Rev. X* **6**, 031006 (2016).
- [60] C. C. Gerry and P. L. Knight, “Quantum superpositions and Schrödinger cat states in quantum optics,” *American Journal of Physics* **65**, 964–974 (1997).
- [61] Sreenath K. Manikandan and Sofia Qvarfort, “Optimal quantum parametric feedback cooling,” *Phys. Rev. A* **107**, 023516 (2023).
- [62] Alekhya Ghosh, Pardeep Kumar, Christian Sommer, Fidel G. Jimenez, Vivishek Sudhir, and Claudiu Genes, “Theory of phase-adaptive parametric cooling,” *Phys. Rev. A* **107**, 053521 (2023).
- [63] Massimiliano Rossi, David Mason, Junxin Chen, Yeghishe Tsaturyan, and Albert Schliesser, “Measurement-Based Quantum Control of Mechanical Motion,” *Nature* **563**, 53–58 (2018).
- [64] Chris Whittle, Evan D. Hall, Sheila Dwyer, Nergis Mavalvala, Vivishek Sudhir, R. Abbott, A. Ananyeva, C. Austin, L. Barsotti, J. Betzwieser, C. D. Blair, A. F. Brooks, D. D. Brown, A. Buikema, C. Cahillane, J. C. Driggers, A. Effler, A. Fernandez-Galiana, P. Fritschel, V. V. Frolov, T. Hardwick, M. Kasprzak, K. Kawabe, N. Kijbunchoo, J. S. Kissel, G. L. Mansell, F. Matchard, L. McCuller, T. McRae, A. Mullavey, A. Pele, R. M. S. Schofield, D. Sigg, M. Tse, G. Vajente, D. C. Vander-Hyde, Hang Yu, Haocun Yu, C. Adams, R. X. Adhikari, S. Appert, K. Arai, J. S. Areeda, Y. Asali, S. M. Aston, A. M. Baer, M. Ball, S. W. Ballmer, S. Banagiri, D. Barker, J. Bartlett, B. K. Berger, D. Bhattacharjee, G. Billingsley, S. Biscans, R. M. Blair, N. Bode, P. Booker, R. Bork, A. Bramley, K. C. Cannon, X. Chen, A. A. Ciobanu, F. Clara, C. M. Compton, S. J. Cooper, K. R. Corley, S. T. Countryman, P. B. Covas, D. C. Coyne, L. E. H. Datrier, D. Davis, C. Di Fronzo, K. L. Dooley, P. Dupej, T. Etzel, M. Evans, T. M. Evans, J. Feicht, P. Fulda, M. Fyffe, J. A. Giaime, K. D. Giardina, P. Godwin, E. Goetz, S. Gras, C. Gray, R. Gray, A. C. Green, E. K. Gustafson, R. Gustafson, J. Hanks, J. Hanson, R. K. Hasskew, M. C. Heintze, A. F. Helmling-Cornell, N. A. Holland, J. D. Jones, S. Kandhasamy, S. Karki, P. J. King, Rahul Kumar, M. Landry, B. B. Lane, B. Lantz, M. Laxen, Y. K. Lecoeuche, J. Leviton, J. Liu, M. Lormand, A. P. Lundgren, R. Macas, M. MacInnis, D. M. Macleod, S. Márka, Z. Márka, D. V. Martynov, K. Mason, T. J. Massinger, R. McCarthy, D. E. McClelland, S. McCormick, J. McIver, G. Mendell, K. Merfeld, E. L. Merilh, F. Meylahn, T. Mistry, R. Mittleman, G. Moreno, C. M. Mow-Lowry, S. Mozzon, T. J. N. Nelson, P. Nguyen, L. K. Nuttall, J. Oberling, Richard J. Oram, C. Osthelder, D. J. Ottaway, H. Overmier, J. R. Palamos, W. Parker, E. Payne, R. Penhorwood, C. J. Perez, M. Pirello, H. Radkins, K. E. Ramirez, J. W. Richardson, K. Riles, N. A. Robertson, J. G. Rollins, C. L. Romel, J. H. Romie, M. P. Ross, K. Ryan, T. Sadecki, E. J. Sanchez, L. E. Sanchez, T. R. Saravanan, R. L. Savage, D. Schaez, R. Schnabel, E. Schwartz, D. Sellers, T. Shaffer, B. J. J. Slagmolen, J. R. Smith, S. Soni, B. Sorazu, A. P. Spencer, K. A. Strain, L. Sun, M. J. Szczepańczyk, M. Thomas, P. Thomas, K. A. Thorne, K. Toland, C. I. Torrie, G. Traylor, A. L. Urban, G. Valdes, P. J. Veitch, K. Venkateswara, G. Venugopalan, A. D. Viets, T. Vo, C. Vorvick, M. Wade, R. L. Ward, J. Warner, B. Weaver, R. Weiss, B. Willke, C. C. Wipf, L. Xiao, H. Yamamoto, L. Zhang, M. E. Zucker, and J. Zweizig, “Approaching the motional ground state of a 10-kg object,” *Science* **372**, 1333–1336 (2021).
- [65] Christiane P Koch, “Controlling open quantum sys-

- tems: tools, achievements, and limitations,” *Journal of Physics: Condensed Matter* **28**, 213001 (2016).
- [66] Lorenzo Campos Venuti, Domenico D’Alessandro, and Daniel A. Lidar, “Optimal control for quantum optimization of closed and open systems,” *Phys. Rev. Appl.* **16**, 054023 (2021).
- [67] Ronan Gautier, Élie Genois, and Alexandre Blais, “Optimal control in large open quantum systems: the case of transmon readout and reset,” (2024), [arXiv:2403.14765 \[quant-ph\]](https://arxiv.org/abs/2403.14765).
- [68] Alicia B. Magann, Christian Arenz, Matthew D. Grace, Tak-San Ho, Robert L. Kosut, Jarrod R. McClean, Herschel A. Rabitz, and Mohan Sarovar, “From pulses to circuits and back again: A quantum optimal control perspective on variational quantum algorithms,” *PRX Quantum* **2**, 010101 (2021).
- [69] Zhi-Cheng Yang, Armin Rahmani, Alireza Shabani, Hartmut Neven, and Claudio Chamon, “Optimizing variational quantum algorithms using pontryagin’s minimum principle,” *Phys. Rev. X* **7**, 021027 (2017).
- [70] Seraph Bao, Silken Kleer, Ruoyu Wang, and Armin Rahmani, “Optimal control of superconducting qubits using pontryagin’s minimum principle: Preparing a maximally entangled state with singular bang-bang protocols,” *Phys. Rev. A* **97**, 062343 (2018).
- [71] Chungwei Lin, Yebin Wang, Grigory Kolesov, and Uro š Kalabić, “Application of pontryagin’s minimum principle to grover’s quantum search problem,” *Phys. Rev. A* **100**, 022327 (2019).
- [72] Mo Zhou, F. A. Cárdenas-López, Sugny Dominique, and Xi Chen, “Optimal control for open quantum system in circuit quantum electrodynamics,” (2024), [arXiv:2412.20149 \[quant-ph\]](https://arxiv.org/abs/2412.20149).
- [73] Yipei Zhang, Philippe Lewalle, and K. Birgitta Whaley, “Solving k-sat problems with generalized quantum measurement,” (2024), [arXiv:2406.13611 \[quant-ph\]](https://arxiv.org/abs/2406.13611).
- [74] Markus Aspelmeyer, Tobias J. Kippenberg, and Florian Marquardt, “Cavity Optomechanics,” *Rev. Mod. Phys.* **86**, 1391–1452 (2014).
- [75] A. A. Clerk, M. H. Devoret, S. M. Girvin, Florian Marquardt, and R. J. Schoelkopf, “Introduction to Quantum Noise, Measurement, and Amplification,” *Rev. Mod. Phys.* **82**, 1155–1208 (2010).
- [76] Massimiliano Rossi, David Mason, Junxin Chen, and Albert Schliesser, “Observing and Verifying the Quantum Trajectory of a Mechanical Resonator,” *Phys. Rev. Lett.* **123**, 163601 (2019).
- [77] Michael R. Vanner, Igor Pikovski, and M. S. Kim, “Towards Optomechanical Quantum State Reconstruction of Mechanical Motion,” *Annalen der Physik* **527**, 15–26 (2015).
- [78] Amir H. Safavi-Naeini, Jasper Chan, Jeff T. Hill, Thiago P. Mayer Alegre, Alex Krause, and Oskar Painter, “Observation of Quantum Motion of a Nanomechanical Resonator,” *Phys. Rev. Lett.* **108**, 033602 (2012).
- [79] C. F. Ockeloen-Korppi, E. Damskäg, J.-M. Pirkkalainen, A. A. Clerk, M. J. Woolley, and M. A. Sillanpää, “Quantum Backaction Evading Measurement of Collective Mechanical Modes,” *Phys. Rev. Lett.* **117**, 140401 (2016).
- [80] N. S. Kampel, R. W. Peterson, R. Fischer, P.-L. Yu, K. Cicak, R. W. Simmonds, K. W. Lehnert, and C. A. Regal, “Improving Broadband Displacement Detection with Quantum Correlations,” *Phys. Rev. X* **7**, 021008 (2017).
- [81] Christoffer B. Møller, Rodrigo A. Thomas, Georgios Vasilakis, Emil Zeuthen, Yeghishe Taturyan, Mikhail Balabas, Kasper Jensen, Albert Schliesser, Klemens Hammerer, and Eugene S. Polzik, “Quantum Back-Action-Evading Measurement of Motion in a Negative Mass Reference Frame,” *Nature* **547**, 191–195 (2017).
- [82] V. Sudhir, D. J. Wilson, R. Schilling, H. Schütz, S. A. Fedorov, A. H. Ghadimi, A. Nunnenkamp, and T. J. Kippenberg, “Appearance and Disappearance of Quantum Correlations in Measurement-Based Feedback Control of a Mechanical Oscillator,” *Phys. Rev. X* **7**, 011001 (2017).
- [83] T. P. Purdy, R. W. Peterson, and C. A. Regal, “Observation of Radiation Pressure Shot Noise on a Macroscopic Object,” *Science* **339**, 801–804 (2013).
- [84] J. D. Thompson, B. M. Zwickl, A. M. Jayich, Florian Marquardt, S. M. Girvin, and J. G. E. Harris, “Strong Dispersive Coupling of a High-Finesse Cavity to a Micromechanical Membrane,” *Nature* **452**, 72–75 (2008).
- [85] Marco G. Genoni, Ludovico Lami, and Alessio Serafini, “Conditional and Unconditional Gaussian Quantum Dynamics,” *Contemporary Physics* **57**, 331–349 (2016).
- [86] Alessio Belenchia, Luca Mancino, Gabriel T. Landi, and Mauro Paternostro, “Entropy Production in Continuously Measured Gaussian Quantum Systems,” *npj Quantum Information* **6**, 1–7 (2020).
- [87] D. J. Wilson, V. Sudhir, N. Piro, R. Schilling, A. Ghadimi, and T. J. Kippenberg, “Measurement-Based Control of a Mechanical Oscillator at Its Thermal Decoherence Rate,” *Nature* **524**, 325–329 (2015).
- [88] Alex G. Krause, Tim D. Blasius, and Oskar Painter, “Optical Read Out and Feedback Cooling of a Nanoscale Optomechanical Cavity,” (2015), [arXiv:1506.01249 \[physics.optics\]](https://arxiv.org/abs/1506.01249).
- [89] M. Poggio, C. L. Degen, H. J. Mamin, and D. Rugar, “Feedback Cooling of a Cantilever’s Fundamental Mode below 5 mK,” *Phys. Rev. Lett.* **99**, 017201 (2007).
- [90] Dustin Kleckner and Dirk Bouwmeester, “Sub-Kelvin Optical Cooling of a Micromechanical Resonator,” *Nature* **444**, 75–78 (2006).
- [91] Thomas Corbitt, Christopher Wipf, Timothy Bodiya, David Ottaway, Daniel Sigg, Nicolas Smith, Stanley Whitcomb, and Nergis Mavalvala, “Optical Dilution and Feedback Cooling of a Gram-Scale Oscillator to 6.9 mK,” *Phys. Rev. Lett.* **99**, 160801 (2007).
- [92] M. Ringbauer, T. J. Weinhold, L. A. Howard, A. G. White, and M. R. Vanner, “Generation of Mechanical Interference Fringes by Multi-Photon Counting,” *New Journal of Physics* **20**, 053042 (2018).
- [93] C.U. Lei, A.J. Weinstein, J. Suh, E.E. Wollman, A. Kronwald, F. Marquardt, A.A. Clerk, and K.C. Schwab, “Quantum Nondemolition Measurement of a Quantum Squeezed State Beyond the 3 dB Limit,” *Physical Review Letters* **117**, 100801 (2016).
- [94] E. E. Wollman, C. U. Lei, A. J. Weinstein, J. Suh, A. Kronwald, F. Marquardt, A. A. Clerk, and K. C. Schwab, “Quantum Squeezing of Motion in a Mechanical Resonator,” *Science* **349**, 952–955 (2015).
- [95] J.-M. Pirkkalainen, E. Damskäg, M. Brandt, F. Massel, and M. A. Sillanpää, “Squeezing of Quantum Noise of Motion in a Micromechanical Resonator,” *Phys. Rev. Lett.* **115**, 243601 (2015).

- [96] F. Lecocq, J. B. Clark, R. W. Simmonds, J. Aumentado, and J. D. Teufel, “Quantum Nondemolition Measurement of a Nonclassical State of a Massive Object,” *Phys. Rev. X* **5**, 041037 (2015).
- [97] A. Pontin, M. Bonaldi, A. Borrielli, F. S. Cataliotti, F. Marino, G. A. Prodi, E. Serra, and F. Marin, “Squeezing a Thermal Mechanical Oscillator by Stabilized Parametric Effect on the Optical Spring,” *Phys. Rev. Lett.* **112**, 023601 (2014).
- [98] Ralf Riedinger, Andreas Wallucks, Igor Marinković, Clemens Löschnauer, Markus Aspelmeyer, Sungkun Hong, and Simon Gröblacher, “Remote Quantum Entanglement between Two Micromechanical Oscillators,” *Nature* **556**, 473–477 (2018).
- [99] C. F. Ockeloen-Korppi, E. Damskägg, J.-M. Pirkkalainen, M. Asjad, A. A. Clerk, F. Massel, M. J. Woolley, and M. A. Sillanpää, “Stabilized Entanglement of Massive Mechanical Oscillators,” *Nature* **556**, 478–482 (2018).
- [100] Ralf Riedinger, Sungkun Hong, Richard A. Norte, Joshua A. Slater, Juying Shang, Alexander G. Krause, Vikas Anant, Markus Aspelmeyer, and Simon Gröblacher, *Nature* **530**, 313–316 (2016).
- [101] T. A. Palomaki, J. D. Teufel, R. W. Simmonds, and K. W. Lehnert, “Entangling Mechanical Motion with Microwave Fields,” *Science* **342**, 710–713 (2013).
- [102] Alexandre Blais, Arne L. Grimsmo, S. M. Girvin, and Andreas Wallraff, “Circuit quantum electrodynamics,” *Rev. Mod. Phys.* **93**, 025005 (2021).
- [103] James D. Teoh, Patrick Winkel, Harshvardhan K. Babla, Benjamin J. Chapman, Jahan Claes, Stijn J. de Graaf, John W. O. Garmon, William D. Kalfus, Yao Lu, Aniket Maiti, Kaavya Sahay, Neel Thakur, Takahiro Tsunoda, Sophia H. Xue, Luigi Frunzio, Steven M. Girvin, Shruti Puri, and Robert J. Schoelkopf, “Dual-rail encoding with superconducting cavities,” *Proceedings of the National Academy of Sciences* **120**, e2221736120 (2023).
- [104] Kevin S. Chou, Tali Shemma, Heather McCarrick, Tzu-Chiao Chien, James D. Teoh, Patrick Winkel, Amos Anderson, Jonathan Chen, Jacob Curtis, Stijn J. de Graaf, John W. O. Garmon, Benjamin Gudlewski, William D. Kalfus, Trevor Keen, Nishaad Khedkar, Chan U Lei, Gangqiang Liu, Pinlei Lu, Yao Lu, Aniket Maiti, Luke Mastalli-Kelly, Nitish Mehta, Shantanu O. Mundhada, Anirudh Narla, Taewan Noh, Takahiro Tsunoda, Sophia H. Xue, Joseph O. Yuan, Luigi Frunzio, Jose Aumentado, Shruti Puri, Steven M. Girvin, Jr. S. Harvey Moseley, and Robert J. Schoelkopf, “Demonstrating a superconducting dual-rail cavity qubit with erasure-detected logical measurements,” (2023), [arXiv:2307.03169 \[quant-ph\]](https://arxiv.org/abs/2307.03169).
- [105] D.K. Weiss, Shruti Puri, and S.M. Girvin, “Quantum random access memory architectures using 3d superconducting cavities,” *PRX Quantum* **5**, 020312 (2024).
- [106] V. V. Sivak, A. Eickbusch, B. Royer, S. Singh, I. Tsioutsios, S. Ganjam, A. Miano, B. L. Brock, A. Z. Ding, L. Frunzio, S. M. Girvin, R. J. Schoelkopf, and M. H. Devoret, “Real-time quantum error correction beyond break-even,” *Nature* **616**, 50–55 (2023).
- [107] Benjamin L. Brock, Shraddha Singh, Alec Eickbusch, Volodymyr V. Sivak, Andy Z. Ding, Luigi Frunzio, Steven M. Girvin, and Michel H. Devoret, “Quantum error correction of qudits beyond break-even,” (2024), [arXiv:2409.15065 \[quant-ph\]](https://arxiv.org/abs/2409.15065).
- [108] Ryotatsu Yanagimoto, Edwin Ng, Atsushi Yamamura, Tatsuhiro Onodera, Logan G. Wright, Marc Jankowski, M. M. Fejer, Peter L. McMahon, and Hideo Mabuchi, “Onset of non-gaussian quantum physics in pulsed squeezing with mesoscopic fields,” *Optica* **9**, 379–390 (2022).
- [109] Ryotatsu Yanagimoto, Edwin Ng, Marc Jankowski, Rajveer Nehra, Timothy P. McKenna, Tatsuhiro Onodera, Logan G. Wright, Ryan Hamerly, Alireza Marandi, M. M. Fejer, and Hideo Mabuchi, “Mesoscopic ultrafast nonlinear optics—the emergence of multimode quantum non-gaussian physics,” *Optica* **11**, 896–918 (2024).
- [110] Ryotatsu Yanagimoto, Rajveer Nehra, Ryan Hamerly, Edwin Ng, Alireza Marandi, and Hideo Mabuchi, “Quantum nondemolition measurements with optical parametric amplifiers for ultrafast universal quantum information processing,” *PRX Quantum* **4**, 010333 (2023).
- [111] Ryotatsu Yanagimoto, Rajveer Nehra, Edwin Ng, Alireza Marandi, and Hideo Mabuchi, “Engineering cubic quantum nondemolition hamiltonian with mesoscopic optical parametric interactions,” (2023), [arXiv:2305.03260 \[quant-ph\]](https://arxiv.org/abs/2305.03260).
- [112] Ryotatsu Yanagimoto, Tatsuhiro Onodera, Edwin Ng, Logan G. Wright, Peter L. McMahon, and Hideo Mabuchi, “Engineering a kerr-based deterministic cubic phase gate via gaussian operations,” *Phys. Rev. Lett.* **124**, 240503 (2020).
- [113] Karl Kraus and Arno Böhm, *States, Effects, and Operations: Fundamental Notions of Quantum Theory: Lectures in Mathematical Physics at the University of Texas at Austin*, Vol. 190 (Springer-Verlag, New York, Berlin, 1983).
- [114] Crispin Gardiner, *Stochastic Methods: A Handbook for the Natural and Social Sciences* (Springer Berlin, Heidelberg, 2010).
- [115] Crispin Gardiner and Peter Zoller, *Quantum Noise: A Handbook of Markovian and Non-Markovian Quantum Stochastic Methods with Applications to Quantum Optics* (Springer Berlin, Heidelberg, 2010).
- [116] C. W. Gardiner, A. S. Parkins, and P. Zoller, “Wavefunction quantum stochastic differential equations and quantum-jump simulation methods,” *Phys. Rev. A* **46**, 4363–4381 (1992).
- [117] Tathagata Karmakar, *Fundamental Investigations of Quantum and Bandlimited Systems*, Ph.D. thesis (2024).
- [118] Yuchen Wang, Zixuan Hu, Barry C. Sanders, and Sabre Kais, “Qudits and high-dimensional quantum computing,” *Frontiers in Physics Volume 8 - 2020* (2020), [10.3389/fphy.2020.589504](https://doi.org/10.3389/fphy.2020.589504).
- [119] Rosario Fazio, Jonathan Keeling, Leonardo Mazza, and Marco Schirò, “Many-body open quantum systems,” (2025), [arXiv:2409.10300 \[quant-ph\]](https://arxiv.org/abs/2409.10300).
- [120] Samuel L. Braunstein and Peter van Loock, “Quantum information with continuous variables,” *Rev. Mod. Phys.* **77**, 513–577 (2005).
- [121] Wong Eugene and Zakai Moshe, “On the relation between ordinary and stochastic differential equations,” *International Journal of Engineering Science* **3**, 213–229 (1965).
- [122] Eugene Wong and Moshe Zakai, “On the Convergence of Ordinary Integrals to Stochastic Integrals,” *The Annals*

- of *Mathematical Statistics* **36**, 1560–1564 (1965).
- [123] L. S. Pontryagin, V. G. Boltyanskii, R. V. Gamkrelidze, and E. F. Mishchenko, *The Mathematical Theory of Optimal Processes*, 1st ed. (The Macmillan Company, 1964).
- [124] P. T. Cochrane, G. J. Milburn, and W. J. Munro, “Macroscopically distinct quantum-superposition states as a bosonic code for amplitude damping,” *Phys. Rev. A* **59**, 2631–2634 (1999).
- [125] Mazyar Mirrahimi, Zaki Leghtas, Victor V Albert, Steven Touzard, Robert J Schoelkopf, Liang Jiang, and Michel H Devoret, “Dynamically protected cat-qubits: a new paradigm for universal quantum computation,” *New Journal of Physics* **16**, 045014 (2014).
- [126] Julien Niset, Jaromír Fiurášek, and Nicolas J. Cerf, “No-go theorem for gaussian quantum error correction,” *Phys. Rev. Lett.* **102**, 120501 (2009).
- [127] A. Kuzmich, L. Mandel, and N. P. Bigelow, “Generation of spin squeezing via continuous quantum non-demolition measurement,” *Phys. Rev. Lett.* **85**, 1594–1597 (2000).
- [128] Christine Guerlin, Julien Bernu, Samuel Deléglise, Clément Sayrin, Sébastien Gleyzes, Stefan Kuhr, Michel Brune, Jean-Michel Raimond, and Serge Haroche, “Progressive field-state collapse and quantum non-demolition photon counting,” *Nature* **448**, 889–893 (2007).
- [129] Jing Zhang, Yu-xi Liu, Re-Bing Wu, Kurt Jacobs, and Franco Nori, “Quantum feedback: Theory, experiments, and applications,” *Physics Reports* **679**, 1 (2017).
- [130] Charlene Ahn, H. M. Wiseman, and G. J. Milburn, “Quantum error correction for continuously detected errors,” *Phys. Rev. A* **67**, 052310 (2003).
- [131] Razieh Mohseninia, Jing Yang, Irfan Siddiqi, Andrew N. Jordan, and Justin Dressel, “Always-On Quantum Error Tracking with Continuous Parity Measurements,” *Quantum* **4**, 358 (2020).
- [132] Joachim Cohen and Mazyar Mirrahimi, “Dissipation-induced continuous quantum error correction for superconducting circuits,” *Phys. Rev. A* **90**, 062344 (2014).
- [133] José Lebreuilly, Kyungjoo Noh, Chiao-Hsuan Wang, Steven M. Girvin, and Liang Jiang, “Autonomous quantum error correction and quantum computation,” (2021), [arXiv:2103.05007 \[quant-ph\]](https://arxiv.org/abs/2103.05007).
- [134] Qian Xu, Guo Zheng, Yu-Xin Wang, Peter Zoller, Aashish A. Clerk, and Liang Jiang, “Autonomous quantum error correction and fault-tolerant quantum computation with squeezed cat qubits,” *npj Quantum Information* **9**, 1–11 (2023).
- [135] Camille Grange, Michael Poss, and Eric Bourreau, “An introduction to variational quantum algorithms for combinatorial optimization problems,” *Annals of Operations Research* **343**, 847–884 (2024).
- [136] William K. Wootters, “Entanglement of formation of an arbitrary state of two qubits,” *Phys. Rev. Lett.* **80**, 2245–2248 (1998).
- [137] Philippe Lewalle, Cyril Elouard, Sreenath K. Manikandan, Xiao-Feng Qian, Joseph H. Eberly, and Andrew N. Jordan, “Entanglement of a pair of quantum emitters via continuous fluorescence measurements: a tutorial,” *Adv. Opt. Photon.* **13**, 517–583 (2021).
- [138] Vincent P. Flynn, Emilio Cobanera, and Lorenza Viola, “Topology by dissipation: Majorana bosons in metastable quadratic markovian dynamics,” *Phys. Rev. Lett.* **127**, 245701 (2021).
- [139] Vincent P. Flynn, Emilio Cobanera, and Lorenza Viola, “Topological zero modes and edge symmetries of metastable markovian bosonic systems,” *Phys. Rev. B* **108**, 214312 (2023).
- [140] Gideon Lee, Tony Jin, Yu-Xin Wang, Alexander McDonald, and Aashish Clerk, “Entanglement phase transition due to reciprocity breaking without measurement or postselection,” *PRX Quantum* **5**, 010313 (2024).
- [141] Hector Hutin, Pavlo Bilous, Chengzhi Ye, Sepideh Abdollahi, Loris Cros, Tom Dvir, Tirth Shah, Yonatan Cohen, Audrey Bienfait, Florian Marquardt, and Benjamin Huard, “Preparing schrödinger cat states in a microwave cavity using a neural network,” *PRX Quantum* **6**, 010321 (2025).
- [142] Riccardo Porotti, Vittorio Peano, and Florian Marquardt, “Gradient-ascent pulse engineering with feedback,” *PRX Quantum* **4**, 030305 (2023).
- [143] Kevin Reuer, Jonas Landgraf, Thomas Fösel, James O’Sullivan, Liberto Beltrán, Abdulkadir Akin, Graham J. Norris, Ants Remm, Michael Kerschbaum, Jean-Claude Besse, Florian Marquardt, Andreas Wallraff, and Christopher Eichler, “Realizing a deep reinforcement learning agent for real-time quantum feedback,” *Nature Communications* **14**, 7138 (2023).
- [144] Pranav Vaidhyathan, Florian Marquardt, Mark T. Mitchison, and Natalia Ares, “Quantum feedback control with a transformer neural network architecture,” (2024), [arXiv:2411.19253 \[quant-ph\]](https://arxiv.org/abs/2411.19253).
- [145] Matteo Puviani, Sangkha Borah, Remmy Zen, Jan Olle, and Florian Marquardt, “Non-markovian feedback for optimized quantum error correction,” *Phys. Rev. Lett.* **134**, 020601 (2025).
- [146] Inés de Vega and Daniel Alonso, “Dynamics of non-markovian open quantum systems,” *Rev. Mod. Phys.* **89**, 015001 (2017).
- [147] Peter Groszkowski, Alireza Seif, Jens Koch, and A. A. Clerk, “Simple master equations for describing driven systems subject to classical non-Markovian noise,” *Quantum* **7**, 972 (2023).
- [148] Daniel Appelo and Yingda Cheng, “Kraus is king: High-order completely positive and trace preserving (cptp) low rank method for the lindblad master equation,” (2024), [arXiv:2409.08898 \[math.NA\]](https://arxiv.org/abs/2409.08898).
- [149] Neal H. McCoy, “On commutation formulas in the algebra of quantum mechanics,” *Transactions of the American Mathematical Society* **31**, 793–806 (1929).
- [150] W.H. Press, S.A. Teukolsky, W.T. Vetterling, and B.P. Flannery, *Numerical Recipes: The Art of Scientific Computing*, 3rd ed. (Cambridge University Press, 2007).
- [151] Kathryn A. Dowland, “Some experiments with simulated annealing techniques for packing problems,” *European Journal of Operational Research* **68**, 389–399 (1993).
- [152] James Bradbury, Roy Frostig, Peter Hawkins, Matthew James Johnson, Chris Leary, Dougal Maclaurin, George Necula, Adam Paszke, Jake VanderPlas, Skye Wanderman-Milne, and Qiao Zhang, “JAX: composable transformations of Python+NumPy programs,” (2018).
- [153] Karmakar Tathagata, “CDJ-P Monitored Oscillator Quantum Optimal Control Codes,” (2025).